HHS Public Access

Author manuscript

Brain Behav Immun. Author manuscript; available in PMC 2022 February 01.

Published in final edited form as:

Brain Behav Immun. 2022 February ; 100: 10–24. doi:10.1016/j.bbi.2021.11.007.

Brain innate immune response *via* miRNA-TLR7 sensing in polymicrobial sepsis

Lin Zou[a,1], **Junyun He**[a,1], **Lili Gu**[a], **Rami A. Shahror**[a], **Yun Li**[a], **Tuoxin Cao**[a], **Sheng Wang**[a], **Jing Zhu**[a], **Huang Huang**[a], **Fengqian Chen**[a], **Xiaoxuan Fan**[b], **Junfang Wu**[a,c,*], **Wei Chao**[a]

[a]Department of Anesthesiology and Center for Shock Trauma Anesthesiology Research, University of Maryland School of Medicine, Baltimore, MD 21201, USA

[b]Center for Innovative Biomedical Resources, University of Maryland School of Medicine, Baltimore, MD 21201, USA

[c]University of Maryland Center to Advanced Chronic Pain Research, University of Maryland, Baltimore, MD 21201, USA

Abstract

Sepsis-associated encephalopathy (SAE) occurs in sepsis survivors and is associated with breakdown of the blood–brain barrier (BBB), brain inflammation, and neurological dysfunction. We have previously identified a group of extracellular microRNAs (ex-miRNAs), such as miR-146a-5p, that were upregulated in the plasma of septic mice and human, and capable of inducing potent pro-inflammatory cytokines and complements. Here, we established a clinically relevant mouse model of SAE and investigated the role of extracellular miRNAs and their sensor Toll-like receptor 7 (TLR7) in brain inflammation and neurological dysfunction. We observed BBB disruption and a profound neuroinflammatory responses in the brain for up to 14 days post-sepsis; these included increased pro-inflammatory cytokines production, microglial expansion, and peripheral leukocyte accumulation in the CNS. In a battery of neurobehavioral tests, septic mice displayed impairment of motor coordination and neurological function. Sepsis significantly increased plasma RNA and miRNA levels for up to 7 days, such as miR-146a-5p. Exogenously added miR-146a-5p induces innate immune responses in both cultured microglia/astrocytes and

*Corresponding author at: University of Maryland School of Medicine, Baltimore, MD 21201, USA. junfang.wu@som.umaryland.edu (J. Wu).

[1]L.Z. and J.H. contributed equally to this work.

Authors contributions

LZ contributed to study conception and design, performed the CLP, IV injection, flow cytometry, miRNA and mRNA qRT-PCR, data analysis, prepared figures, wrote the manuscript; JH performed BBB permeability and data analysis, ICV injection, the qPCR and quantification, cell isolation for flow cytometer, manuscript preparation; L.G. performed the CLP, miRNA treatment, qRT-PCR and the cytokines ELISA; RAS and YL performed all behavioral tests and data analysis; TC performed primary microglia and astrocytes cultures, WB and quantification; JZ and HH performed the CLP and assisted with the flow cytometry; SW and FC performed miRNA and mRNA qRT-PCR, and data analysis; XF assisted the flow cytometry experiments; JW contributed to study conception and design, data analysis for behavior, wrote the manuscript, revised figures; WC contributed to study conception and design, data analysis, edited the manuscript and figures. All authors read and approved the manuscript prior to submission.

Declaration of Competing Interest

The authors declare that they have no known competing financial interests or personal relationships that could have appeared to influence the work reported in this paper.

Appendix A. Supplementary data

Supplementary data to this article can be found online at https://doi.org/10.1016/j.bbi.2021.11.007.

the intact brain *via* a TLR7-dependent manner. Moreover, mice genetically deficient of miR-146a showed reduced accumulation of monocytes and neutrophils in the brain compared to WT after sepsis. Finally, ablation of TLR7 in the $TLR7^{-/-}$ mice preserved BBB integrity, reduced microglial expansion and leukocyte accumulation, and attenuated GSK3β signaling in the brain, but did not improve neurobehavioral recovery following sepsis. Taken together, these data establish an important role of extracellular miRNA and TLR7 sensing in sepsis-induced brain inflammation.

Keywords

Sepsis; Encephalopathy; Innate immunity; Extracellular RNA; MicroRNA; TLR7; Neuroinflammation; IL-6; Cytokines; Behavior

1. Introduction

Sepsis is a serious clinical condition with life-threatening organ dysfunction mediated by a dysregulated host response to invading pathogens (Singer et al., 2016). Up to 70% of septic patients develop cerebral dysfunction (Fleischmann et al., 2016), a condition termed sepsis-associated encephalopathy (SAE), which is the most common cause of encephalopathy in medical-surgical ICU (BLECK et al., 1993). Clinical studies have shown that septic patients with acute encephalopathy have higher mortality rate (49%) than patients with normal mental status (26%) (Sprung et al., 1990). Moreover, among sepsis survivors, many developed long-term cognitive impairment that adversely impacts the quality of their lives (Annane and Sharshar, 2015; Chung et al., 2020; Gofton and Young, 2012; Widmann and Heneka, 2014).

The pathogenesis of SAE has not been well established, but several likely mechanisms have been proposed; these include microscopic brain injury, impaired blood–brain barrier (BBB) function and cerebral microcirculation, altered cerebral metabolism and neurotransmission, and brain inflammation (Gofton and Young, 2012; Widmann and Heneka, 2014). Profound systemic and tissue inflammation is a hallmark of sepsis and plays a critical role in the pathogenesis and early mortality of sepsis (Angus and van der Poll, 2013; Hotchkiss et al., 2016). During sepsis, the host innate immunity is markedly activated in response to pathogen invasion with massive neutrophil/monocyte activation, cytokine storm, complement activation, coagulation activation, and tissue apoptotic and necrotic cell death (Angus and van der Poll, 2013). A recent postmortem analysis of brain tissue in septic patients identified that innate immune activation was closely associated with brain pathologies, especially expression of primary cytokines, complement factors, and DAMP (Bustamante et al., 2020). Brain inflammation reportedly increases amyloid-β peptide (Aβ) levels and contributes to cognitive impairment (Annane and Sharshar, 2015; Glass et al., 2010; Gofton and Young, 2012; Schwalm et al., 2014). While both clinical and animal data suggest the role of brain inflammation in SAE, the molecular mechanisms leading to cerebral inflammation and neurocognitive dysfunction are not well understood.

microRNAs (miRNAs) are a group of small and single-stranded noncoding RNAs. The primary role of cellular miRNAs is to regulate gene expression by binding to the 3′ untranslated region of the target mRNAs, resulting in degradation of mRNA and inhibition

of translation. However, emerging studies have revealed that miRNAs widely exist outside of cells in the blood circulation (Chen et al., 2008; Chim et al., 2008; Lawrie et al., 2008; Mitchell et al., 2008; Xu et al., 2018) and body fluids (Hanke et al., 2010; Kosaka et al., 2010; Weber et al., 2010). These extracellular miRNAs (ex-miRNAs) can act on the recipient cells in a paracrine/ endocrine fashion and play an important role in various pathological conditions (Fabbri et al., 2012; Lehmann et al., 2012; Park et al., 2014; Turchinovich et al., 2016). We and others have recently demonstrated that certain uridine-rich miRNAs including miR-146a, miR-34a, miR-122, and miR-145 are released into the blood during sepsis and myocardial ischemic injury in animals (Feng et al., 2015; Feng et al., 2017; Zou et al., 2016) and patients (Caserta et al., 2016). These ex-miRNAs are highly pro-inflammatory promoting innate immune activation through the nucleic acid sensing by TLR7 (Feng et al., 2015; Feng et al., 2017; Xu et al., 2018; Zou et al., 2016), a dual receptor for uridine/guanosine and single-stranded small RNA (Zhang et al., 2016). Furthermore, mice lacking TLR7 showed reduced circulatory inflammation, alleviated kidney injury, attenuated coagulopathy, and improved sepsis survival (Jian et al., 2019; Williams et al., 2019), demonstrating the role of single-stranded RNA sensing in sepsis pathogenesis. However, the role TLR7 signaling in brain inflammation and dysfunction in sepsis is unknown.

In this study, we established a clinically relevant mouse model of SAE following highly inflammatory bacterial peritonitis as featured by a significant disruption of the BBB, marked brain immune cell recruitment and microglial activation, and neurological dysfunction. Using genetic and pharmacological approaches, we delineated the innate proinflammatory effects of miR-146a-5p and TLR7 signaling in microglia cultures *in vitro* and the intact brain *in vivo*, and explored the role of ex-miRNAs-TLR7 signaling in the pathogenesis of SAE.

2. Materials and methods

2.1. Animals

Eight to sixteen-week old male mice were used in current study. Wild-type (WT) C57BL/6J mice (stock No. 000664) were purchased from Jackson Laboratories (Bar Harbor, ME) and housed at least 2 weeks in our animal facility prior to experiment. TLR7 knockout (KO, TLR7$^{-/-}$) mice (Tlr^{tm1Flv}/J, stock No. 008380) and miR-146a KO (miR-146 a$^{tm1.1Bal}$/J, stock No. 016239) were initially purchased from Jackson Laboratories and bred in the animal facilities of University of Maryland School of Medicine with 12 h dark and 12 h light cycles. The mice were fed with autoclaved food. All experimental procedure on animals were performed in accordance with protocols approved by the Institutional Animal Care and Use Committee at the University of Maryland School of Medicine. All animal experiments were performed in compliance with the relevant guidelines and regulations of the National Institutes of Health (Bethesda, MD) and the ARRIVE guidelines of the National Centre for the Replacement, Refinement, and Reduction of Animals in Research (London, EN).

2.2. Polymicrobial sepsis model in mice

Cecal ligation and puncture (CLP) procedure was performed as previously described (Jian et al., 2019; Zou et al., 2010). In brief, mice were anesthetized by intraperitoneal injection

of ketamine (100 mg/kg) and xylazine (4 mg/kg). After disinfection, abdominal cavity was opened in layers. The feces in the cecum was milked to the distal end and the cecum was ligated at 1.5 cm position from the end. Two holes was made in the cecum using 18-gauge needle and 1–2 mm feces was squeezed out before returning to the peritoneal cavity. The abdominal cavity was then closed in layers with 5–0 silk sutures and prewarmed saline (30 μl/g body weight) was administrated subcutaneously. Analgesia was given following the protocol as previously described (Jian et al., 2019). Of note, in the studies involving different mouse strains, the operators (LZ, LG, JZ, and HH) were blinded to strain information.

2.3. RNA extraction and qRT-PCR

2.3.1. mRNA expression in the brain—Both TaqMan- and SYBR Green-based detection were applied in qRT-PCR. RNA was isolated using Trizol (Sigma, SIG-T9724). A total of 1 μg RNA was transcribed to cDNA using M-MLV reverse transcriptase (Promega, M1705). Quantitative real-time PCR was performed using GoTaq SYBR qPCR master kit (Promega, A6001, Madison, WI) as described previously (Li et al., 2020; Zou et al., 2016). The PCR primer sequences are listed below: GAPDH (Forward: 5′-AACTTTGGCATTGTGGAAGG-3′, Reverse:5′ GGATGCAGGGATGATGTTCT-3′); IL-1β (Forward: 5′GCCCATCCTCTGTGACTCAT-3′, Reverse: 5′-AGGCCACAGGTATTTTGTCG-3′), IL-6 (Forward: 5′-AGTTGCCTTCTTGGGACTGA-3′, Reverse: 5′-TCCACGATTTCCCAGAGAAC-3′), CXCL2 (Forward: 5′-CCGCTGTTGTGGCCAGTGAACTGCG-3′, Reverse 5′TTAGCCTTGCCTTTGTTCAGTAT3′), TNFα (Forward: 5′CTGGGACA GTGACCTGGACT-3′, Reverse: 5′-GCACCTCAGGGAAGAGTCTG-3′). For Taqman assay, qRT-PCR amplification was performed using cDNA TaqMan Universal Master Mix II (Applied Biosystems/Thermos Fisher Scientific, 4440047, Waltham, MA). TaqMan Gene Expression assays for following mouse genes were performed: GAPDH (Mm99999915_g1), IL-4αR (Mm012751 39_m1), SOCS3 (Mm01249 143_g1), Chil3 (Mm00657889_mH), CD206 (Mm01329362_m1), TGFβ (Mm01178820_m1), Arg-1 (Mm00475988_m1), TNFα (Mm004432 58_m1), IL-1β (Mm00434228_m1), CXCL2 (Mm0043 6450_m1), IL-6 (Mm00446190_m1). Transcript expression was calculated using the comparative Ct method normalized to GPDAH ($2^{-\Delta\Delta}$Ct) and expressed as the fold change in the treatment group over the control.

2.3.2. miRNA expression in the brain—RNA was reversed transcribed using a miScript II RT kit (Qiagen, 218161, Germantown, MD). Brain miR-146a-5p and U6 was quantified by miScript SYBR Green PCR kit (Qiagen, 218073, Germantown, MD) and corresponding primers (Qiagen, Germantown, MD) following the manufactory's instruction. Relative miRNA expression was calculated using the comparative Ct method normalized to U6 and expressed as the fold change in the treatment group over the control.

2.3.3. miRNA expression in the plasma—After adding cel-miR-39 control (Qiagen, Germantown, MD) to plasma samples, RNA was isolated using Trizol LS (Thermo Fisher Scientific, Waltham, MA) from 200 μl of EDTA-anticoagulated plasma and quantified by Quanti-iT RNA assay kit (Thermo Fisher Scientific). Plasma miRNAs and spike-in cel-miR-39 were quantified with miRCURY LNA RT and miRCURY SYBR GREEN PCK kits

using corresponding following the manufactory's instruction. Relative miRNA expression was calculated using the comparative Ct method normalized to spike-in cel-miR-39 and expressed as the fold change in the treatment group over the control. To determine plasma miRNA copy number, qPCR standard curves were generated with serially diluted cDNA solutions (from 10^4 to 10^{10} copies/μl).

2.4. Flow cytometry

At the designed time point, mice were euthanized and perfused with 50 ml saline via left ventricle of the heart at a perfusion rate of 5 ml/min. The isolated cerebral cortex and hippocampus were placed in complete RPMI 1640 media (Gibco, 11–875–119, Waltham, MA) and mechanically and enzymatically digested in the buffer containing collagenase/dispase (40 μg/ml; Roche Diagnostics/Sigma, 10269638001), papain (0.6 U/ml; Worthington Biochemical corporation, LS003126), EDTA (1 mM; Invitrogen/Thermo Fisher Scientific, 15575020), and DNase I (0.6 mg/ml; Roche Diagnostics/Sigma, 10104159001, St. Louis, MO) for 1 h at 37 °C on a shaking incubator (200 rpm). The cell suspension was washed and filtered through a 70 μM cell strainer followed by 30%/70% isopercoll (Sigma, GE17–0891-01, St. Louis, MO) gradient isolation (Li et al., 2020; Ritzel et al., 2020). The isolated mononuclear cells were manually counted using hematocytometer and then stained with viability dye of Zombie red (1:500, Biolegend, 423109,) or Zombie NIR (1:100, Biolegend, 423105, San Diego, CA) for 10 min on ice. The cells were washed and incubated with CD16/CD32 Fc blocker (0.5 μg/sample, Invitrogen, Thermo Fisher Scientific, 14–0161-85, clone 93) on ice for 10 min prior to the staining of the following antibodies: CD45-efluro 450 (1:120, Invitrogen, Thermo Fisher Scientific, 48–0451-80, clone 30-F11), CD11b-APC-efluo780 (1:480, Invitrogen, Thermo Fisher Scientific, 47–0112-82, clone M1/70), Ly6G-BV421 (1:500, BD Biosciences, 562737, clone 1A8), Ly6C-PE (1:500, Biolegend, 128007, clone HK1.4) at 4 °C for 30 min. The cells were then fixed and permeabilized using intracellular fixation & permeabilization buffer (Invitrogen, Thermo Fisher Scientific, 88–8824-00) following the manufactory's instruction and incubated with intracellular cytokine antibodies including TNFα-FITC (1:100, BD Biosciences, 554418, clone MP6-XT22), IL-1β-PerCP-efluro 710 (1:100, Invitrogen, Thermo Fisher Scientific 46–7114-82, clone NJTEN3) and IL-6-APC (1:100, Biolegend, 504508, clone MP5–20F3) at room temperature for 30 min. Fluorescence minus one (FMO) control was applied to determine the gating strategy for intracellular cytokines. Data was acquired on a LSR II (BD Biosciences, San Jose, CA) or Aurora flow cytometer (Cytek Bioscience, Fremont, CA), and analyzed by FlowJo (BD Biosciences, San Jose, CA).

2.5. BBB permeability assay

The BBB permeability was assessed as described previously (Kuriakose et al., 2018) with modification. In brief, 100 μl sodium fluorescein (NaF, 376 Da, Sigma, F6377, 100 mg/ml in PBS) was administered via the lateral tail vein. Thirty minutes later, mice were euthanized and 200 μl blood was collected. Following perfusion of 80 ml saline from left ventricle of heart, cortex and hippocampus were carefully dissected, weighted, and then homogenized in 1:5 vol of PBS. Supernatant of brain homogenates were collected after centrifugation at 10,000 g for 15 min at 4 °C. Sera and supernatants from the brain homogenates were then processed as follows: equal volume of 15 % trichloroacetic acid was added to the

supernatant and serum, respectively. After centrifugation, the supernatant from the brain homogenates was neutralized with 1/5 vol of 5 N NaOH. The fluorescence was measured at excitation/emission of 485/528 nm and concentration of NaF was calculated using a standard curve. The permeability was determined as the ratio of NaF of the supernatant from the brain homogenates over the sera. The comparison was expressed as the ratio of CLP/Sham control.

2.6. Neurobehavioral testing

The following behavior tests were performed as previously described (Li et al., 2020; Matyas et al., 2017; Ritzel et al., 2021; Ritzel et al., 2020; Wu et al., 2016) during 1 to 5 weeks post-surgery with strain and group information blinded to the operators. To minimize stress and fatigue, each test was performed on a different day.

2.6.1. Motor function—(1) The spontaneous locomotor activity was examined by open field (OF) test. Mice were placed in a corner facing the wall of the OF chamber (22.5 × 22.5 cm) and allowed to explore the chamber freely for 5 min. Total distance travelled (m), mean speed (m/s), and time immobility were recorded by the computer-based ANY-maze automated video-tracking system (Stoelting). (2–3) Fine motor coordination was assessed using a beam walk (BW) test and the CatWalk. In the BW test, mice were placed on one end of a wooden beam (120 mm in length and 5 mm wide), and the number of foot faults of the right hindlimb were recorded over 50 steps. Mice were trained every day on the BW for 3 days prior to the surgery. Gait analysis was performed using the CatwalkXT automated system (Noldus; RRID:SCR_004074). Mice were first placed in the open end of the CatWalk under the red ceiling light and allowed to walk across the walkway to the darkened escape enclosure. A minimum of three valid runs, or complete walkway crossings, were obtained for each mouse. The following variables including regularity index (the percentage of step cycles that can be characterized as fitting a standard pattern of gait), stride length (the distance between steps of a single hindpaw), print position (the distance between the hind and forepaw of one side during gait), and phase dispersions-diagonal (mean ipsilateral phase dispersion values from left front paw and right hind paw was measured within a step cycle) were analyzed. (4) The accelerating Rotorod was performed to assess the gross motor function and balance (Doran et al., 2019). Mice were placed on the rod which accelerated from 4 to 60 RPM with maximal speed reached within 20 s. Latency to fall from the rod was recorded and the scores in each mouse were averaged from the three trials. A 5–10 min rest period in the home cage with access to food and water was allowed between each trial.

2.6.2. Cognitive function—The Y-maze and novel objective recognition (NOR) were performed to evaluate spatial working memory and nonspatial hippocampal-mediated memory. (1) The Y-maze (Stoelting) was built of black plastic and consisted of three identical arms, each arm 38.1 cm long, 5 cm wide, and 12.7 cm high, at an angle of 120° with respect to the other arms. One arm was randomly selected as the “start” arm. The mouse was placed into the end of the “start” arm and allowed to explore the maze freely for 6 min. The arm entries (arms A–C) were recorded using ANY-maze software. An arm entry was counted when all four paws of the mouse entered the arm. An alternation was

designated when the mouse entered three different arms consecutively. The percentage of alternation was calculated using the following equation: total alternations × 100/(total arm entries −2). If a mouse scored significantly greater than 50% alternations (the chance level for choosing the unfamiliar arm), this was indicative of functional working memory. (2) In the NOR test, mice were habituated in the OF chamber for 5 min. After 24 h, mice were placed into the same OF chamber containing two identical objects near the left and right corners. During the training (sample) phase, mice were allowed to explore freely until they spent a total of 30 s exploring the objects (exploration was recorded when the front paws or nose contacted the object). Mice were then returned to their home cages. After 24 h, object recognition was tested by substituting a novel object for a familiar training object (novel object location counterbalanced across mice). Time spent with each object was recorded. Because mice inherently prefer to explore novel objects, a preference for the novel object [more time than chance (15 s) spent with the novel object] indicates intact memory for the familiar object.

2.6.3. The novelty-suppressed feeding (NSF), the tail-suspension (TS), and the forced swim (FS)—These tests were performed to assess rodent behaviors in septic mice. (1) The NSF measures a rodent's aversion to eating in a novel environment. After fasting for 24 h (with ad lib access to water), mice were habituated for 2 h in a brightly lit room. A piece of food chow was placed in the center of the chamber and the mice were placed in a corner of the chamber, facing the wall. The time to reach food was recorded as latency. If the mouse failed to eat the food within 10 min, the mouse was considered to have failed the test. Upon returning to their home cage, the time to reach food was recorded and the ratio of latency in open field and the home cage was calculated. (2) The TS test is based on the observation that an immobile posture develops when the mice is placed in an inescapable hemodynamics stress of being hung by their tail. Each mouse was suspended at a height of 50 cm using adhesive tape placed approximately 1 cm from the tip of its tail. The duration of immobility was recorded throughout the 5-min test period. (3) The FS test is performed to assess the state of immobility when placing an animal in a container filled with water, which may be considered to reflect a measure of behavioral despair. Animals were placed in transparent plastic cylinder (45 cm high × 20 cm diameter) filled with water (23 ± 2 °C; 28 cm in depth) for 6 min. The duration of immobility was recorded.

2.6.4. Social interaction test—This task is based on rodent's innate tendency to investigate a novel congener over a familiar one (Moy et al., 2004). This test utilizes a rectangular box made from clear plexiglass, divided into three equal-sized chambers at 20 (width) × 40 (length) × 23 (height) cm. Access to the two side chambers from the center chamber is allowed by 7 × 7 cm doors, which can be closed when needed. Two metal wired cup-like containers were used to hold the 2 stimulus mice. The experiment consists of three sequential 10-minute stages: (1) habituation: the test mouse is allowed to freely explore all three chambers for a time period of 10 min and habituate to the novel environment; (2) exposure to novel stimulus mouse 1: a stimulus mouse and an object of interest randomly assigned to either the left or right chamber, which the mouse the again allowed to explore for a duration of 10 min; and (3) the object is exchanged for a second, novel stimulus mouse. Measured outcomes included time spent in each chamber and time spent exploring each

mouse. Sociability was calculated as % of time of mouse/(time of mouse + time of object). Preference for social novelty was calculated as % of time of novel mouse/(time of novel mouse + time of familiar mouse).

2.7. Primary microglia and astrocyte culture and treatment

Primary microglia and astrocytes were cultured from the cerebral cortex of neonatal mice as described (Li et al., 2021; Matyas et al., 2017). Briefly, cortices from both WT and TLR7$^{-/-}$ pups were dissected in chilled HBSS, and single cell suspensions were distributed in poly-D-lysine (PDL) precoated T75 flasks. Cells were cultured in DMEM/F12 (Invitrogen, 1132033, Waltham, MA) media, supplemented with 10% fetal bovine serum (FBS, Gibco/Thermo Fisher Scientific, 10–082-147, Waltham, MA) and 2% peniciline/streptomycine (Corning, 30–002-cl, Waltham, MA) at 37 °C with 5% CO_2. Once cells had grown to confluence, the flaks were shaken at 200 rpm for several days and microglia and astrocyte were separated and cultured for specified experiments.

Mature single-stranded miRNA mimics with phosphorothioate linkages including miR-34a-5p, miR-122–5p, miR-145–5p, miR-146a-5p, and miR-146a-5p mutant (U → A) were synthesized by Integrated DNA Technologies (Coralville, IA) and suspended in sterile DEPC H_2O. The miRNA sequences were provided by miRB 22.1 (http://www.mirbase.org/) and reported previously (Zou et al., 2016). Microglia and astrocytes were starved in serum-free media for 1 h and 24 h, respectively, followed by treatment with 50 nM of various miRNA mimics complexed with lipofectamine 3000 (Thermo Fisher Scientific, L3000015, Waltham, MA), R837 (InvivoGen, San Diego, CA), and poly I:C (Enzo Life Sciences, Farmingdale, NY) for additional 16–18 h. Media were then collected and stored at −80 °C for future ELISA analysis.

2.8. Elisa

Cytokines in the media were analyzed using commercially available mouse CXCL2 and IL-6 DuoSet ELISA kit from R&D Systems (DY 406, DY452, Minneapolis, MN) following the manufactory's instruction.

2.9. Intracerebroventricular (ICV) injection

WT and TLR7$^{-/-}$ mice received a single ICV injection of single-stranded miR-146a-5p (5 μg) complexed with lipofectamine 3000 or lipofectamine control. In detail, the prepared reagents were injected into the left ventricle of the brain using stereotactic coordinates as previous described (Khan et al., 2021; Sabirzhanov et al., 2014) and set up as follows: from bregma = anteroposterior, −0.5 mm; mediolateral, −1.0 mm; dorsoventral, −2.0 mm. The injection was achieved by using a 30-gauge needle attached to a Hamilton syringe at a rate of 0.5 μl/min, with a final volume of 5 μl. The operator (JH) was blinded to both reagent and strain information.

2.10. Western blot

Western blot was performed as previously described with minor modification (Li et al., 2021; Ritzel et al., 2021). After whole body perfusion, cerebral cortex and hippocampus were homogenized in NP-40 buffer supplemented with protease and phosphatase inhibitor

(Roche Diagnostics/Sigma, St. Louis, MO). Protein quantitation was performed using BCA method and 20 μg protein lysate fractionated by SDS-PAGEs. Membranes were blotted with the following antibodies: GAPDH (1:3000, Biolegend, 919501), and rabbit anti-mouse phosphor (Ser21/9)-GSK3α/β (1:1000, Cell Signaling, 8566, Danvers, MA). Protein was visualized using SuperSignal West Dura Extend Duration Substrate (Pierce/Thermo Fisher, Waltham, MA) and images were acquired in a ChemiDoc system (Bio-Rad Laboratories, Hercules, CA). The intensity was quantified using the NIH Image J program. The intensity of phospho-GSK3β was normalized to total GSK3β and then expressed as fold change to WT/sham.

2.11. Statistical analysis

Age and gender matched mice were allocated to different experimental groups. Operators for CLP (LG, JZ, LZ and HH) and ICV (JH) were blinded to strain information and treatment. Behavioral tests (RAS and YL) and data analysis (JW) were blinded to group allocation. All analysis of the experimental outcomes was performed with coding system prior to revealing of strain or treatment information. No statistical power calculation was conducted before the current study. Sample sizes were estimated based on previous similar studies and our preliminary data. Specific comparisons were made based on scientific hypotheses for the study. Statistical analyses were performed using GraphPad Prism 9 software (GraphPad Software Inc., USA). Normality of all numerical data was assessed using D'Agostino-Pearson test or Kolmogorov-Simirnov test. A parametric test was used if the hypothesis of normality was not rejected. Nonparametric Mann–Whitney U tests were applied to the data that did not pass normality test. For multiple group comparison, one-way or two-way ANOVA with Bonferroni *post hoc* test was applied when the data met the two assumptions-normal population distribution and equal variance. If the data did not meet the assumptions, we performed ANOVA analysis after the data were transformed to be the log format or Kruskal-Wallis test. Data were presented as mean ± SEM unless stated otherwise. The null hypothesis was rejected for $p < 0.05$ with two tails.

3. Results

3.1. Polymicrobial sepsis induces marked brain innate immune response in mice

We created a polymicrobial sepsis model in adult male mice following cecal ligation and puncture. In this animal sepsis model, most deaths occur within the first week (Muenzer et al., 2006; Rittirsch et al., 2009). Mice are died of septic shock and organ injury due to excessive inflammatory response in this stage. Mice survived from the early hyperinflammatory stage will then enter immunosuppressive phase whereas most of them die of secondary infections.

Twenty-four hours after sham or CLP procedures, the cerebral cortex and hippocampus were dissected for assessment of inflammatory markers. qRT-PCR analysis showed that the proinflammatory cytokines TNF-α and IL-1β transcripts increased approximately 5.2-fold ($t_{(14)} = 3.860$, $p = 0.0017$ *vs.* sham, *t* test) and 2.8-fold ($t_{(14)} = 2.233$, $p = 0.0424$ *vs.* sham, *t* test), respectively, in cerebral cortex in response to CLP challenge (Fig. 1A). CXCL2, a potent neutrophil chemoattractant, was markedly increased with approximate

318-fold elevation in CLP mice ($p = 0.0002$ *vs.* sham, Mann-Whitney *U* test). A similar proinflammatory cytokine response pattern was observed in the hippocampus ($t_{(14)} = 3.842$, $p = 0.0018$ for TNF-α, *t* test; $p = 0.0052$ for IL-1β, Mann-Whitney *U* test; $p = 0.0002$ for CXCL2 Mann-Whitney *U* test, *vs.* sham; Fig. 1A. CLP mice also exhibited an increase in several key anti-inflammatory cytokines, including IL-4αR ($t_{(14)} = 7.506$, $p < 0.0001$ for cortex and $t_{(14)} = 8.947$, $p < 0.0001$ for hippocampus, *t* test), SOCS3($t_{(14)} = 4.528$, p = 0.0005 for cortex and $t_{(14)} = 7.099$, p < 0.0001for hippocampus, *t* test), Chitinase-like protein 3 (Chil3, $t_{(14)} = 2.858$, $p = 0.0127$ for cortex and $t_{(13)} = 4.107$, $p = 0.0012$ for hippocampus, *t* test) in both cortex and hippocampus as compared to sham mice (*t* test, Fig. 1B). However, the anti-inflammatory genes CD206 and TGF-β in CLP mice were significantly reduced to 43.6% ($t_{(14)} = 2.774$, $p = 0.0149$) and 22.5% ($t_{(14)} = 3.494$, $p = 0.0036$), respectively, of the sham mice in the cortex.

Next, we examined peripheral myeloid cell accumulation and microglial expansion in the brain hemisphere at 24 h and 14 days post-surgery. Both myeloid ($CD45^{high}/CD11b^{+}$) and microglial ($CD45^{mid}/CD11b^{+}$) cells express CD45 and CD11b and they were separated by different expression level of CD45 (Li et al., 2020; Ritzel et al., 2021). The gating strategy and representative flow images are shown in Fig. S1A–C. In the acute phase of sepsis at 24 h, the number of microglia augmented in the septic brain (sham *vs.* CLP: 81.8 ± 19.0 *vs.* 184.2 ± 22.5 × 10^3, $t_{(19)} = 3.159$, $p = 0.0052$, *t* test, Fig. 1C), indicating an activation of local immune environment. The number of monocytes/macrophages (Mϕ) ($CD45^{high}CD11b^{+}Ly6C^{+}Ly6G^{-}$) in the septic brain was 9-fold ($p < 0.0001$, Mann-Whitney *U* test) higher than that of sham brain. The neutrophils ($CD45^{high}CD11b^{+}Ly6C^{low}Ly6G^{+}$) numbers increased 3.5-fold ($p = 0.0042$, Mann-Whitney *U* test) in response to CLP (Fig. 1C). There was no difference in the number of lymphocytes in the brain between sham and CLP groups (sham *vs.* CLP: 3.76 ± 1.7 *vs.* 3.78 ± 1.9 × 10^3). Surprisingly, at 14 days after CLP, when systemic inflammation was largely resolved (Gasparotto et al., 2018), myeloid cells including monocytes/Mϕ and neutrophils displayed a sustained increase in the CLP brain ($t_{(8)} = 8.677$, $p < 0.0001$, *t* test) whereas microglia numbers went back to the level of sham mice (Fig. 1D). Moreover, flow cytometry analysis of intracellular cytokines (Fig. S1D–E) showed that the number of microglial and myeloid cells producing IL-1β, a mediator of synaptic dysfunction in sepsis (Moraes et al., 2015), was significantly higher in CLP than sham mice (Fig. 1E). We did not observe, however, any differences in the % of IL-6^{+} microglia or myeloid cells between sham and CLP mice. While the % of TNFα^{+} microglia remained unchanged. CLP caused a reduction of TNFα^{+} myeloid cells at 14 d post-CLP ($t_{(8)} = 2.626$, $p = 0.0304$, Fig. 1E. Finally, we examined the BBB integrity in the brain of both sham and CLP mice by i.v. administration of sodium fluorescein (NaF), a highly sensitive low molecular weight (MW) inert tracer for determining the breakdown of microvessels in the CNS (Kuriakose et al., 2018). The amount of NaF entering the brain from the blood circulation was 1.43-fold ($t_{(16)} = 2.489$, $p = 0.0242$) and 1.70-fold ($t_{(16)} = 3.975$, $p = 0.0011$), respectively, in the cortex and hippocampus of CLP mice relative to the sham control (Fig. 1F). All together, these results indicate that polymicrobial sepsis induces an acute as well as a sustained brain innate immune inflammation in mice.

3.2. Polymicrobial sepsis impairs diverse neurobehavioral function in mice

To assess whether the mouse model of polymicrobial sepsis leads to neurological dysfunction, we performed comprehensive neurobehavioral tests for motor, cognition, and mood status at one to four weeks after surgical procedures. The diagram in Fig. 2A illustrates the experimental timeline for the battery of various neurobehavioral tests in three major categories in sham and CLP mice that survived initial sepsis.

All mice (CLP at eight-week-old) survived in sham group and the survival rate of CLP group was 36% at week 1 and continued to week 4. Determination of spontaneous locomotor activity at 1 week post-CLP using the open-field test showed that sepsis resulted in a significantly reduced distance traveled ($t_{(14)} = 4.578$, $p = 0.0035$, *t* test) and walking speed ($t_{(14)} = 4.632$, $p = 0.0004$, *t* test) as compared with sham mice (Fig. 2B). In addition, septic mice displayed increased immobility time ($t_{(14)} = 4.044$, $p = 0.0012$, *t* test) suggesting reduced exploratory behavior. However, at 4 weeks after CLP, the differences in the open field test between sham and sepsis mice disappeared (Fig. 2C). We next examined gait dynamics using the CatWalk apparatus, which measures the kinematic properties of locomotion. Phase dispersion measures the coordinated walking pattern. The mean phase dispersion values from left front paw to right hind paw was measured within a step cycle. CLP resulted in reduction in the phase dispersion at week 1 ($t_{(8.322)} = 1.686$, $p = 0.0644$, *t* test), however, 1.84-fold higher at week 4 ($t_{(8.629)} = 1.895$, $p = 0.046$, *t* test) than that in sham cohort (Fig. 2D), indicating a greater asynchrony in paw movement. There were no apparent differences in the regularity index, stride length, or print position between sham and CLP groups (data not shown). Furthermore, mice were tested for fine motor coordination and balance on the beam walk at 1 and 4 weeks post-CLP. The number of paw slips (foot fault) showed a slightly increase at week 1, however, significantly elevated at week 4 ($t_{(14)} = 2.215$, $p = 0.0438$, *t* test) following CLP procedure as compared with sham cohort (Fig. 2E).

Next, we evaluated the long-term effects of sepsis on cognitive behavior. Non-spatial retention memory was tested by a Novel Objective Recognition (NOR) at both week 1 and week 4 post-surgery. During training (Sample phase), all mice spent equal time with two identical subjects in the left and right position (left panel in Fig. 2F–G), indicating an intact memory. No significant differences in choice phase were observed between the sham and CLP groups at 1 week after sepsis (right panel in Fig. 2F). At 4 weeks post-operation, while CLP mice spent reduced time with the novel object 24 h after training ($F_{(1,28)} = 9.874$, $p = 0.0691$; Two-way ANOVA, right panel in Fig. 2G compared with the sham-injured group, the differences did not reach statistical significance. Furthermore, hippocampus-dependent spatial working memory was evaluated by the Y-maze spontaneous alternation test at 1 week and 4 weeks post-surgery. There were no apparent differences in the percentage of spontaneous alteration between sham and CLP groups (Fig. 2H–I), indicative of a preserved spatial working memory. Y maze testing revealed a transient decrease in total arm entries at 1 week post-CLP ($t_{(14)} = 2.996$, $p = 0.0096$, *t* test), correlated with impaired spontaneous locomotor activity.

To investigate whether sepsis causes persistent changes in feeding and stress behaviors, we measured rodent performance in Novelty Suppressed Feeding (NSF) and Tail suspension

(TS) tests. Mouse presents an inhibition of feeding behavior caused by exposure to a novel environment. NSF is to measure the time until the mice expresses a feeding behavior to a novel environment, which illustrated as latency. As shown in Fig. 2J–K, the latency in novel arena remained unchanged between sham and CLP groups at week 1 while significantly increased in CLP mice at week 4 ($t_{(13)} = 2.596$, $p = 0.0222$, *t* test), implying a development of suppressed feeding behavior in the chronic phase of sepsis. During tail suspension test, there were no apparent differences in the immobility time between sham and CLP groups at 1 week post-injury. However, chronic CLP mice displayed greater immobility at 4 weeks post-injury ($t_{(13)} = 1.672$, $p = 0.0592$, *t* test, Fig. 2L.

Collectively, these data show that mice that survived initial septic shock displayed various deficits in fine motor function and performed poorly in the NOR, NSF, and TS tests, at 7 and 28 days after CLP, indicating sepsis-mediated neurological dysfunction.

3.3. Extracellular miRNAs induce glial activation in vitro and in vivo

In our previous study, quantitative RT-PCR and miRNA array analysis revealed an increase in bacterial 16 s rRNA and multiple host miRNAs (*e.g.,* miR-145–5p, miR-146a-5p, miR-122–5p) in the blood following CLP (Zou et al., 2016). Recently, using unbiased small RNA sequencing, we profiled plasma RNA in mice and humans, and identified that more than 80% of plasma RNAs were host-derived RNAs and 70% were miRNAs. There were distinct miRNA expression patterns between sepsis and health (data not shown). One of the most abundant and upregulated plasma miRNAs in sepsis at 24 h is single-stranded miR-146a-5p. To further characterize plasma extracellular miRNAs in sepsis, we collected plasma at day 1, 7, and 14 following CLP (Fig. 3A). CLP led to an elevation of plasma RNA concentration at day 1 (day 1 *vs.* sham; 325 ± 87 *vs.* 131 ± 12, ng/mL), which peaked at day 7 (575 ± 88, ng/mL) ($F_{(3.16)} = 6.957$, $p = 0.0033$, One-way ANOVA; d 7 *vs.* sham, $p = 0.0026$, *post hoc* Bonferroni test) followed by a decrease at day 14 (d 14 *vs.* d 7, $p = 0.0398$, one-way ANOVA*, post hoc* Bonferroni test). We also tested the expression of a group of miRNAs (miR-146a, miR-34a, miR-122, miR-145) in the plasma. CLP led to a rising of plasma miR-146a-5p and miR-145–5p at day 1 with fold-change of 4.9 ± 0.7 ($F_{(3.16)} = 12.19$, $p = 0.0001$, one-way ANOVA; d1 *vs.* sham, $p = 0.0001$, *post hoc* Bonferroni test), and 4.5 ± 1.0 ($F_{(3,16)} = 10.96$, $p = 0.0004$, one-way ANOVA; d1 *vs.* sham, p = 0.0028, *post hoc* Bonferroni test), respectively (Fig. 3B). Plasma miR-122 also elevated following CLP but the increase did not reach statistical significance.

To explore the role of ex miRNAs in brain innate immune response, we tested the function of microRNAs detected above in mouse microglia and astrocyte cultures. As shown in Fig. 3C, microglia responded to exogenously added miR-146a-5p mimic with marked productions of CXCL2 ($F_{(4,10)} = 188.9$, $p < 0.0001$, one-way ANOVA, *vs.* Lipo) and IL-6 ($F_{(4,10)} = 326.5$, $p < 0.0001$, one-way ANOVA, *vs.* Lipo). Other three miRNAs were tested at the same concentrations but exhibited much lower levels of cytokine production (Fig. 3C). The effect of miR-146a-5p in microglia was dose- and uridine-dependent as U → A mutation (miR-146a-mutant) completed abolish the effect (treatment effect, $F_{(1,16)} = 162.9$, $p < 0.0001$ for CXCL2 and $F_{(1,16)} = 80.14$, $p < 0.0001$ for IL-6; two-way ANOVA *post hoc* Bonferroni test, Fig. 3D). In comparison to microglia, astrocytes also responded

to miR-146a-5p but with a much lower level of CXCL2 production ($F_{(4,10)} = 59.89$, $p = 0.0001$, one-way ANOVA, *vs.* Lipo, Fig. 3E.

We further examined whether ex-miR-146a-5p was sufficient to induce brain inflammation *in vivo via* local delivery. As shown in Fig. 4A, intracerebroventricular (ICV) injection of 5 μg of miR-146a induced marked increase in multiple cytokine gene expression including *Il-1β*, *Il-6*, *Tnfα* and chemokine CXCL2 in both cerebral cortex ($t_{(4.239)} = 2.758$, $p = 0.0478$ for *Il-1β*; $t_{(4.147)} = 2.727$, $p = 0.0506$ for *Il-6*; $t_{(4.024)} = 2.651$, $p = 0.0566$ for *Tnfα*, *vs.* sham, *t* test) and hippocampus ($t_{(4.014)} = 3.162$, $p = 0.034$ for *Il-1β*; $t_{(4.217)} = 2.771$, $p = 0.0474$ for *Il-6*; $t_{(4.382)} = 8.035$, $p = 0.009$ for *Cxcl2*; $t_{(4.158)} = 3.419$, $p = 0.0252$ for *Tnfα*, *vs.* sham, *t* test) at 24 h. Flow cytometry analysis within the same time frame revealed a robust increase in the numbers of microglia (Lipofectamine *vs.* miR-146a, 35.6 ± 9.8 *vs.* 107.4 ± 29.7 × 10^3, $t_{(8)} = 2.298$, $p = 0.05$, *t* test), monocytes/ Mϕ (Lipofectamine *vs.* miR-146a, 1.7 ± 0.5. *vs.* 155.6 ± 33.6 × 10^3, $t_{(4.002)} = 4.585$, $p = 0.0101$, *t* test) and neutrophils (Lipofectamine *vs.* miR-146a, 0.33 ± 0.07. *vs.* 36 ± 8.9 × 10^3, $t_{(4.000)} = 3.971$, $p = 0.0165$, *t* test) in the brain (Fig. 4B, Fig. S2A) following miR-146a-5p injection. Moreover, the number of microglia and myeloid cells expressing IL-1β was also significantly increased at 2.66-fold ($t_{(8)} = 3.264$, $p = 0.0115$, *t* test) and 1.46-fold ($t_{(8)} = 2.676$, $p = 0.0281$, *t* test), respectively (Fig. 4C, Fig. S2B). Taken together, these data suggest that direct ICV injection of miR-146a-5p induced a robust local cytokine production and innate immune cell activation.

3.4. miR-146a-5p induces brain innate immune activation via TLR7

To determine the signaling pathway through which miR-146a-5p causes the brain immune activation, we examined the effects of TLR7 and TLR3, the two pattern-recognition receptors sensing single- and double-stranded RNA, respectively (Fitzgerald and Kagan, 2020; Roers et al., 2016). As illustrated in Fig. 5A, loss of TLR7, but not TLR3, abolished miR-146a-5p ($F_{(2,30)} = 543.6$, $p < 0.0001$, two-way ANOVA *post hoc* Bonferroni test) and R837 (a known TLR7 agonist) ($F_{(2,30)} = 543.6$, $p < 0.0001$, two-way ANOVA *post hoc* Bonferroni test) -induced CXCL2 production in cultured microglia, suggesting a TLR7-dependent mechanism. In contrast, poly I:C-induced response was abolished in microglial cells deficient of TLR3, but remained the same in TLR7-deficient cells. Interestingly, we also observed a much higher (370 fold) TLR7 gene expression in microglia than that in astrocytes (Fig. 5B), which could explain a more robust cytokine response in microglia than astrocytes in response to miR-146a-5p or R837 (Fig. 5A, Fig. 3C–E). To identify the role of TLR7 in mediating miR-146a-induced brain inflammation *in vivo*, miR-146a-5p was administrated into intact brain by ICV injection in WT and $TLR7^{-/-}$ mice. Twenty-four hours later, the isolated cerebral cortex and hippocampus were analyzed for expression of miR-146a-5p, cytokines, and immune cells. There was a comparable level of miR-146a-5p expression in the cortex between WT and $TLR7^{-/-}$ mice since the Ct numbers did not differ between the two groups (Fig. 5C). However, in the cortex, there was a significantly lower levels of IL-6 ($t_{(12)} = 3.046$, $p = 0.0102$, *t* test) and TNF-α ($t_{(12)} = 3.412$, $p = 0.0052$, *t* test) gene expression in $TLR7^{-/-}$ mice as compared to that of WT following miR-146a-5p administration (Fig. 5D). In the hippocampus, we only observed a difference in TNF-α production between WT and $TLR7^{-/-}$ cortex ($t_{(12)} = 3.653$, $p = 0.0033$, *t* test, Fig. 5D). While the number of microglial cells were similar in WT and $TLR7^{-/-}$ mice following

miR-146a-5p injection (Fig. 5E), the percentage of microglia producing intracellular TNFα was significantly reduced in TLR7$^{-/-}$ mice compared to that of WT mice ($t_{(12)} = 4.029$, $p = 0.0017$, *t* test, Fig. 5F, Fig. S2B). Moreover, there was a significant reduction in neutrophils ($t_{(12)} = 3.394$, $p = 0.0053$, *t* test) and monocytes/ Mϕ ($t_{(12)} = 4.516$, $p = 0.0007$, *t* test) in the brains of TLR7$^{-/-}$ mice compared with that of WT mice (Fig. 5G). And the myeloid cells in TLR7$^{-/-}$ mice had lower intracellular expression of Il-1β ($t_{(12)} = 5.772$, $p < 0.0001$, *t* test) and IL-6 ($t_{(12)} = 4.416$, $p = 0.0008$, *t* test) relative to WT control after miR-146a-5p injection (Fig. 5H, Fig. S2B).

3.5. miR-146a knockout mice display fewer monocytes and neutrophils in the septic brain

Next, we took a loss-of-function approach and tested the role of endogenous miR-146a in brain inflammation by using mice genetically deficient of miR-146a (Boldin et al., 2011). Twenty-four hours following CLP procedure, miR-146a KO mice had a higher rectal core temperature than that of WT (31.4 ± 1.1 *vs.* 27.2 ± 1.3 °C, $t_{(24.93)} = 2.443$, $p = 0.022$, *t* test, Fig. 6A, suggesting a less severe circulatory shock in these mice. Of note, no difference in rectal temperature was observed between WT and miR-146a KO sham mice (37.1 ± 0.37 *vs.* 37.2 ± 0.25 °C). In addition, miR-146a KO mice also improved the survival in mice of severe sepsis (data not shown). Similar to what we observed in the previous experiments, there was a significant increase in monocytes and neutrophils in the brain of septic WT mice. In comparison, septic miR-146a-KO mice presented significantly fewer monocytes/ Mϕ and neutrophils in both absolute number (monocyte: $F_{(1,38)} = 4.408$, $p = 0.0519$, two-way ANOVA *post hoc* Bonferroni test; neutrophil: $F_{(1,38)} = 10.03$, $p < 0.0001$, two-way ANOVA *post hoc* Bonferroni test after log transformation, Fig. 6B–D and percentage (monocytes/Mϕ: $F_{(1,38)} = 6.250$, $p = 0.0196$, two-way ANOVA *post hoc* Bonferroni test; neutrophil: $F_{(1,38)} = 6.620$, $p = 0.0343$, two-way ANOVA *post hoc* Bonferroni test after log transformation, Fig. 6B–D in the brain. These data suggest that loss of miR-146a mitigates brain inflammatory response during sepsis.

3.6. TLR7$^{-/-}$ mice had improved BBB integrity and reduced brain inflammation in sepsis

Given the importance of TLR7 in miR-146a-5p sensing in the brain, we next tested the role of TLR7 in sepsis-induced BBB impairment and brain inflammation. To test BBB integrity, septic mice were injected via tail vein with sodium fluorescein, and cerebral cortex and hippocampus were dissected for BBB permeability assay at 24 h post-sham or CLP procedure. As illustrated in Fig. 7A, septic WT mice had a significant increase in BBB permeability in both cortex and hippocampus compared with the sham mice. In comparison, septic TLR7$^{-/-}$ mice exhibited no difference in the BBB permeability compared to their sham controls, suggesting a preservation of the BBB integrity in the septic TLR7$^{-/-}$ mice ($F(1,13) = 7.183$, $p = 0.0261$ for cortex and $F(1,13) = 10.88$, $p = 0.0120$ for hippocampus; two-way ANOVA followed by Bonferroni multiple comparisons test). Moreover, qPCR analysis of the whole brain lysates revealed that septic WT mice had an increase in mRNA expression of IL-1β ($F(1,20) = 1.574$, $p = 0.0377$), TNF-α ($F(1,20) = 7.702$, $p = 0.0009$), IL-6 ($F(1,20) = 3.523$, $p = 0.0087$), IL-4αR ($F(1,20) = 12.65$, $p = 0.0006$) and Chil3 ($F_{(1,20)} = 9.043$, $p = 0.0082$; by two-way ANOVA *post hoc* Bonferroni test) compared with their sham controls. In comparison, TLR7$^{-/-}$ mice had attenuated proinflammatory cytokine gene responses (IL-1β ($F(1,20) = 3.458$, $p = 0.0325$), TNF-α ($F(1,20) = 5.326$, $p = 0.0075$), IL-6

($F_{(1,20)}$ = 5.783, p = 0.0119; two-way ANOVA Bonferroni *post hoc* test) (Fig. 7B. Flow cytometry demonstrated that mice deficient of TLR7 had significantly lower numbers of microglia (WT-CLP *vs.* TLR7$^{-/-}$-CLP, 65.7 ± 10.3 *vs.* 26.7 ± 3.4 × 10^3, $F_{(1,16)}$ = 15.06, p = 0.0012), and monocytes ($F_{(1,16)}$ = 9.493, p = 0.0013) and neutrophils ($F_{(1,16)}$ = 13.33, p = 0.0003, Fig. 7C, Fig. S2C in the brain. On day 14, WT mice that survived initial septic shock exhibited unchanged microglial cells, but 3.4-fold in monocytes (Ly6C$^+$Ly6G$^-$, $F_{(1,18)}$ = 25.11, p < 0.0001), and 6.4-fold in neutrophils (Ly6C^{low}Ly6G$^+$, $F_{(1,18)}$ = 30.16, p < 0.0001) in the brain as compared to WT sham mice (Fig. 7D, Fig. S2D. In comparison to septic WT mice, septic TLR7$^{-/-}$ mice had a marked reduction in brain myeloid cells including monocytes ($F_{(1,18)}$ = 8.096, p = 0.0011) and neutrophils ($F_{(1,18)}$ = 13.65, p < 0.001; two-way ANOVA followed Bonferroni *post hoc* test, Fig. 7C–D, Fig. S2C–D. All together, these data suggest that TLR7 mediates inflammatory signals that controls brain microglia and myeloid cells following septic shock.

In human peripheral blood monocytes, TLR-mediated cytokine production, *e.g.,* IL-1β, IL-6, and TNFα, is reportedly regulated by glycogen synthase kinase 3 (GSK3) *via* PI3 kinase-Akt pathway (Martin et al., 2005). To determine the intracellular signaling by which TLR7 mediates brain inflammation during sepsis, we assessed GSK3β phosphorylation/ activation in the brain following sepsis. At 24 h post-CLP, Western blot analysis (Fig. 7E–F revealed that septic WT mice had a significant increase in GSK3β phosphorylation in both the cortex ($F_{(1,20)}$ = 8.472, p = 0.0004, two-way ANOVA followed Bonferroni *post hoc* test) and hippocampus regions ($F_{(1,20)}$ = 1.615, p = 0.0031, two-way ANOVA followed Bonferroni *post hoc* test) compared with sham mice. In contrast, the sepsis-induced GSK3β phosphorylation was abolished in TLR7$^{-/-}$ mice, suggesting an essential role of TLR7 signaling in brain GSK3β activation during sepsis.

Finally, we examined the effects of TLR7 on behavioral outcome after sepsis. Age matched 4-month-old male TLR7$^{-/-}$ mice and their WT littermates were subjected to CLP and motor, cognitive recovery, and mood status were assessed before and at 4 weeks post-operation. The overall mortality for this set of behavioral studies was 43% in septic WT mice and 22% in septic TLR7$^{-/-}$ mice (n = 28/group, p < 0.05). At 4 weeks after CLP, there were no differences between all groups in spontaneous locomotor activity, motor balance, and motor coordination (Fig. 8A. Also, CLP did not alter the percentage of spontaneous alterations in the Y-maze test, when compared to sham counterparts, indicative of intact hippocampus-dependent spatial working memory (Fig. 8B. However, CLP caused a significant decrease in total arm entries in both WT and TLR7$^{-/-}$ mice ($F_{(1,57)}$ = 63.87, p < 0.0001, two-way ANOVA *post hoc* Bonferroni test, Fig. 8B. In the NOR test (Fig. 8C, CLP in WT mice significantly decreased time spent with the novel object versus familiar object in a novel object recognition task ($t_{(24)}$ = 2.187, p = 0.0387, *t* test), however, TLR7$^{-/-}$ CLP animals spent even less time with novel objects than WT-CLP ($t_{(33)}$ = 3.473, p = 0.0015, *t* test), suggesting impaired recognition memory in the KO mice following CLP. Given that sham and CLP mice spent equal time interacting with left- and right-side objects during the training phase, our data suggest that CLP induces lasting deficits in short-term recognition memory and preference for novelty in both WT and TLR7 KO mice. There were no apparent differences in the forced swim and tail suspension tests (Fig. 8D–E as well as sociability and preference for social exploration (Fig. 8F between two groups at 4 weeks post-CLP. Taken

together, these data suggest that while TLR7 deletion preserves BBB integrity and reduces neuroinflammatory signaling in the brain, it fails to improve long-term neurological recovery after sepsis.

4. Discussion

In a clinically relevant animal model of polymicrobial sepsis, we demonstrated an acute brain inflammation within 24 h of CLP evidenced by active cytokine production, increased microglia and myeloid cells including monocytes/neutrophils, and BBB disruption. Some of these proinflammatory changes including brain monocytes/neutrophils accumulation and intracellular cytokine expression sustained for at least 14 days and were associated with a neurological dysfunction, which replicate some of the clinical presentations of human SAE (Gofton and Young, 2012). Extracellular single-stranded miR-146a-5p, abundant and upregulated in the plasma of septic mice and humans, proved to be highly proinflammatory and induced a dose-dependent cytokine production in microglia and astrocytes in cultures and brain innate immune responses in intact animals *via* TLR7 nucleic acid sensing pathway. Moreover, we discovered that lack of endogenous miR-146a appeared attenuating brain innate immune cell accumulation induced by polymicrobial sepsis. Finally, we demonstrated that the extracellular miRNA sensor TLR7 was important in mediating sepsis-induced pathological changes consistent with acute brain inflammation. These included BBB impairment, proinflammatory gene expression, microglial expansion, monocyte/neutrophil brain accumulation and activation. Although CLP mice performed poorly in the NOR task, we did not see significant improvement of behavioral outcome in TLR7$^{-/-}$ septic mice despite attenuated acute brain inflammation in these mice. Taken together, our study established a clinically relevant mouse model of sepsis-associated encephalopathy and demonstrated a pivotal role of extracellular miR-146a-5p and TLR7 sensing in brain innate immune responses during polymicrobial sepsis.

We identified impaired BBB function and marked brain inflammation as evidenced by multiple pro-inflammatory cytokine gene expression in cerebral cortex and hippocampus, microglial expansion and activation, and myeloid immune cell influx. Sustained brain inflammation up to 14 days was associated with impairment of neurological function examined in a battery of behavioral tests at 7 days and 4 weeks in septic mice. Multiple factors may contribute to the chronic behavioral changes in these septic animals. The proinflammatory mediators such as TNF-α, IL-1β, and IL-6 reportedly act directly on neurons and induce neurodegenerative changes in the brain (McCoy and Tansey, 2008; Simi et al., 2007). IL-1β, a critical cytokine sustaining neuroinflammation, was reportedly associated with cognitive impairment after sepsis (Mina et al., 2014; Moraes et al., 2015). In addition to cytokines and consistent with previous studies (Andonegui et al., 2018; Singer et al., 2016), we observed a persistent peripheral myeloid cell infiltration and microglia activation in the brain, which served as another key factor contributing to neuroinflammation. Meanwhile, we also observed a robust chemokine CXCL2 expression in the brain at 24 h. We speculate that activated and expanded microglia may release chemokines, which lead to myeloid cell recruitment to and persistent presence in the septic brain. Even though their numbers returned to the sham level at 14 days, together with accumulating monocytes/neutrophils, these microglial cells showed a capacity to produce

proinflammatory cytokines and may contribute to the chronic brain inflammation. It is worth noting that those mice that survived the initial septic shock exhibited a minor impact of fine motor coordination but a major impairment of mood status and cognitive dysfunction at 4 weeks after the initial polymicrobial infection, which is consistent with the behavior presentation from human septic survivors (Annane and Sharshar, 2015; Gofton and Young, 2012). Collectively, our mouse model closely simulates clinical sepsis-associated encephalopathy in humans as featured by brain inflammation and neurological dysfunction.

Several extracellular miRNAs, *e.g.,* miR-146a, miR-145, miR-34a, miR-122, are found abundant in septic plasma at 24 h post-CLP in mice and septic patients (data not shown), and are capable of activating innate immune responses in macrophages (Feng et al., 2017; Zou et al., 2016) and cardiomyocytes (Shimada et al., 2020). In this study, we demonstrate an increase of plasma RNA and certain uridine-rich miRNAs over the course of 1–14 days post-infection. *In vitro*, we treated cultured microglia and astrocytes with synthetic miR-146a, miR-145, miR-34a, or miR-122, and observed a robust dose-dependent response of IL-6 and CXCL2. Among these ex-miRNAs, exogenous miR-146a presented the most potent pro-inflammatory effects. Moreover, these effects seem to be dependent of the single-stranded RNA sensor TLR7 but not the double-stranded RNA sensor TLR3. We found that TLR7 was predominantly expressed in microglia compared with that in astrocytes. Thus, this may explain that microglia displayed more potent responses to exogenous miR-146a-5p than astrocytes. To further investigate the role of miRNA-TLR7 signaling in brain inflammation *in vivo*, we injected miR-146a-5p into the cerebral ventricle. The local administration of miR-146a-5p replicated the brain inflammation that we observed in the septic brain including elevated proinflammatory cytokines, peripheral neutrophil and monocyte accumulation, and microglial activation. Consistent with our *in vitro* findings, these proinflammatory effect in the intact brain appeared mediated by TLR7 as genetic lack of TLR7 substantially reduced cytokine expression, myeloid cell accumulation, and microglial activation. Together, these studies demonstrate that stimulation of miR-146a-5p → TLR7 pathway is sufficient to activate brain innate immune response *in vitro* and *in vivo.* Under systemic inflammatory condition, extracellular miRNAs may well function as a proinflammatory mediator across blood brain barrier as a part of extracellular EV cargo (Jeyaram et al., 2020; Xu et al., 2018) during sepsis. It has been reported that upon challenged with endotoxin or CLP, there is a marked increase in EVs and several EV-associated proinflammatory miRNAs in the CSF, including miR-146a and miR-155 (Balusu et al., 2016). These EVs and their cargo miRNAs may cross the leaky ependymal cell layer that lines the ventricles and are taken up by astrocytes and microglia, where they initiate proinflammatory responses (Balusu et al., 2016). Other studies have reported a pivotal role of TLR7 in neurodegeneration *via* its sensing of extracellular miRNAs. For example, miR let-7b activates neuronal TLR7 and causes neuronal cell death (Lehmann et al., 2012) and mediates pain (Park et al., 2014). miR let-7b also activates TLR7 in murine microglia leading to increase secretion of TNF-α (Buonfiglioli et al., 2019; Lehmann et al., 2012). Our study unraveled yet another function of miRNAs in the CNS as a TLR7 activator promoting brain innate immune inflammation.

We investigated the role of TLR7 sensing in sepsis-triggered brain inflammation and found that TLR7-deficient mice had significantly reduced brain inflammation as evidenced by

mitigated cytokine transcripts, attenuated peripheral neutrophil/monocyte influx, limited microglial expansion, and, importantly, preserved BBB barrier function during the acute phase of sepsis. Based on the current findings and our previous studies (Jian et al., 2019; Williams et al., 2019), we speculate that absence of TLR7 signaling led to attenuated brain inflammation probably *via* both peripheral and central mechanisms. Our previous study has revealed that TLR7 knockout mice exhibit attenuated plasma cytokines including IL-6, TNF-α, and CXCL2 (Jian et al., 2019). Circulating cytokines can comprise BBB integrity or enter the brain directly (Varatharaj and Galea, 2017), and subsequently activate microglia. Hence, the reduction in systemic cytokines in TLR7$^{-/-}$ mice may limit the amounts of inflammatory cytokines entering the brain. Alternatively, absence of TLR7 in the brain cells such as microglia may limit the proinflammatory signaling initiated by local brain extracellular miRNAs as demonstrated in the direct miR-146a-5p injection experiments and by others (Balusu et al., 2016). The reduced local cytokine response in the brain, as a result, attenuated the peripheral leukocyte infiltration and diminished the correspondent damage. Furthermore, loss of TLR7 sensing could also prevent phosphorylation of GSK3β, a proinflammatory intracellular signaling that is reportedly increased in the hypothalamus of septic rat (Santos-Junior et al., 2018). Supporting the critical role of miR-146a-5p → TLR7 signaling in sepsis-induced brain inflammation is the finding that miR-146a-deficiency also led to attenuated accumulation of peripheral myeloid cells such as monocytes and neutrophils in the brain.

The long-term impact of targeting TLR7 on neurological function following sepsis is unknown. In the present study, we did not observe differential changes between Sham-WT and Sham-TLR7$^{-/-}$ mice in locomotor activity, motor coordination and balance, cognition, performance in the forced swim and tail suspension tests, as well as social interaction tests. Depletion of TLR7 did not resolve sepsis-mediated long-term neurological dysfunction. We speculate that the cause of sepsis-mediated neurological dysfunction is multifactorial, resolving brain inflammation alone is insufficient to improve brain functional outcomes. In addition, age when insult occurs, and injury severity may also contribute to the neurological function following sepsis. Eight-week-old mice subjected to CLP showed a 36% survival rate at 4 weeks post-operation. While CLP mice spent reduced time with the novel object 24 h after training compared with the sham-injured group, the differences did not reach statistical significance. Four-month-old WT mice subjected to CLP displayed a 67% survival rate at 4 weeks post-operation. We found that CLP mice spent comparably less time with novel objects than sham animals. Given that sham and CLP mice spent equal time interacting with left- and right-side objects during the training phase, our data suggest that CLP induces lasting deficits in short-term recognition memory and preference for novelty. Whether or not age and injury severity affect CLP-mediated brain neuroinflammation and outcome have not been reported which is intriguing for future research.

Gender-related differences after sepsis have been reported with respect to higher mortality and organ failure, and poor cognition in male compared to their female counterparts (Diodato et al., 2001; Schroder et al., 1998). Sex differences in mice were seen in the hippocampal response after acute CLP (Barter et al., 2019). In order to minimize variability of experimental outcomes affected by female hormones and to reduce number of animals to reach statistical significance only male mice were chosen for this study. Sex differences

in CLP-mediated brain neuroinflammation have not been reported which is intriguing for future investigation.

Another limitation of the study is our inability to differentiate the location of monocyte/neutrophils between CNS parenchyma and CNS interface (*e.g.,* subdural meninges choroid plexus, and perivascular space) using flow cytometry. While flow cytometry has an advantage to detect multiple cell types simultaneously and quantitatively, it loses the spatial resolution. Nevertheless, given that multiple evidence suggests a role of CNS interface in propagation of inflammation to CNS parenchyma in response to systemic inflammatory stimuli (Balusu et al., 2016; Engelhardt et al., 2001; Shimada and Hasegawa-Ishii, 2021), inclusion of innate immune cells near the CNS interface in our flow cytometry study should not decrease the significance of the finding. Finally, how miR-146a crosses the BBB and activates brain TLR7 during sepsis warrants future study. Systemic administration of extracellular vesicles can influence CNS function (Lino et al., 2021; Xin et al., 2013), suggesting a possible route of extracellular vehicles across the BBB and moving from the peripheral circulation to the CNS. Future direction of targeting extracellular vesicles as a miRNA cargo will be carefully investigated.

In summary, in a mouse model of polymicrobial sepsis, we demonstrated acute and chronic brain inflammation and long-term impairment of neurological function. Activation of extracellular miR-146a-5p → TLR7 signaling was sufficient to stimulate microglia, astrocytes, and intact brain to promote a potent innate immune response in the CNS. Taking a loss-of-function approach, we identified a contributory role of endogenous miR-146a and TLR7 sensing in animal SAE. Hence, our study suggested extracellular miRNA sensing via TLR7 as a possible link of neuroinflammation within the brain microenvironment during polymicrobial sepsis.

Supplementary Material

Refer to Web version on PubMed Central for supplementary material.

Acknowledgments

This work was supported by grants from the National Institutes of Health (R01NS110567 to WC, JW, and LZ, R01GM117233, R01GM122908, R35GM140822 to WC, R01NS110825, R01NS110635, R01NS094527, and RF1NS110637 to JW, R35GM124775 to LZ), Frontiers in Anesthesia Research Award from International Anesthesia Research Society (WC), and Faculty Research Award from Shock Society (LZ). We thank Lulu Liu and Hui Li for help with primary cell cultures and mouse perfusion, and Ping Cui for assistance in flow cytometry.

References

Andonegui G, Zelinski EL, Schubert CL, Knight D, Craig LA, Winston BW, Spanswick SC, Petri B, Jenne CN, Sutherland JC, Nguyen R, Jayawardena N, Kelly MM, Doig CJ, Sutherland RJ, Kubes P, 2018. Targeting inflammatory monocytes in sepsis-associated encephalopathy and long-term cognitive impairment. JCI Insight 3.

Angus DC, van der Poll T., 2013. Severe sepsis and septic shock. N. Engl. J. Med. 369 (9), 840–851. [PubMed: 23984731]

Annane D, Sharshar T, 2015. Cognitive decline after sepsis. Lancet Respir. Med. 3 (1), 61–69. [PubMed: 25434614]

Balusu S, Van Wonterghem E, De Rycke R, Raemdonck K, Stremersch S, Gevaert K, Brkic M, Demeestere D, Vanhooren V, Hendrix A.n., Libert C, Vandenbroucke RE, 2016. Identification of a novel mechanism of blood-brain communication during peripheral inflammation via choroid plexus-derived extracellular vesicles. EMBO Mol. Med. 8 (10), 1162–1183. [PubMed: 27596437]

Barter J, Kumar A, Stortz JA, Hollen McKenzie, Nacionales D, Efron PA, Moldawer LL, Foster TC, 2019. Age and Sex Influence the Hippocampal Response and Recovery Following Sepsis. Mol. Neurobiol. 56 (12), 8557–8572. [PubMed: 31278440]

Bleck Thomas P., Smith Michael C., Pierre-Louis Serge J.-C., Jares Joseph J., Murray Joan, Hansen Carolyn.A., 1993. Neurologic complications of critical medical illnesses. Crit. Care Med. 21 (1), 98–103. [PubMed: 8420739]

Boldin MP, Taganov KD, Rao DS, Yang L, Zhao JL, Kalwani M, Garcia-Flores Y, Luong M, Devrekanli A, Xu J, Sun G, Tay J, Linsley PS, Baltimore D, 2011. miR-146a is a significant brake on autoimmunity, myeloproliferation, and cancer in mice. J. Exp. Med. 208, 1189–1201. [PubMed: 21555486]

Buonfiglioli A, Efe IE, Guneykaya D, Ivanov A, Huang Y, Orlowski E, Kruger C, Deisz RA, Markovic D, Fluh C, Newman AG, Schneider UC, Beule D, Wolf SA, Dzaye O, Gutmann DH, Semtner M, Kettenmann H, Lehnardt S, 2019. let-7 MicroRNAs Regulate Microglial Function and Suppress Glioma Growth through Toll-Like Receptor 7. Cell Rep. 29, 3460–3471.e3467. [PubMed: 31825829]

Bustamante AC, Opron K, Ehlenbach WJ, Larson EB, Crane PK, Keene CD, Standiford TJ, Singer BH, 2020. Transcriptomic Profiles of Sepsis in the Human Brain. Am. J. Respir. Crit. Care Med. 201 (7), 861–863. [PubMed: 31940219]

Caserta S, Kern F, Cohen J, Drage S, Newbury SF, Llewelyn MJ, 2016. Circulating Plasma microRNAs can differentiate Human Sepsis and Systemic Inflammatory Response Syndrome (SIRS). Sci. Rep. 6, 28006. [PubMed: 27320175]

Chen X.i., Ba Y.i., Ma L, Cai X, Yin Y, Wang K, Guo J, Zhang Y, Chen J, Guo X, Li Q, Li X, Wang W, Zhang Y, Wang J, Jiang X, Xiang Y, Xu C, Zheng P, Zhang J, Li R, Zhang H, Shang X, Gong T, Ning G, Wang J, Zen K.e., Zhang J, Zhang C-Y, 2008. Characterization of microRNAs in serum: a novel class of biomarkers for diagnosis of cancer and other diseases. Cell Res. 18 (10), 997–1006. [PubMed: 18766170]

Chim SS, Shing TK, Hung EC, Leung TY, Lau TK, Chiu RW, Lo YM, 2008. Detection and characterization of placental microRNAs in maternal plasma. Clin. Chem. 54, 482–490. [PubMed: 18218722]

Chung HY, Wickel J, Brunkhorst FM, Geis C, 2020. Sepsis-Associated Encephalopathy: From Delirium to Dementia? J. Clin. Med. 9.

Diodato MD, Knöferl MW, Schwacha MG, Bland KI, Chaudry IH, 2001. Gender differences in the inflammatory response and survival following haemorrhage and subsequent sepsis. Cytokine 14 (3), 162–169. [PubMed: 11396994]

Doran SJ, Ritzel RM, Glaser EP, Henry RJ, Faden AI, Loane DJ, 2019. Sex Differences in Acute Neuroinflammation after Experimental Traumatic Brain Injury Are Mediated by Infiltrating Myeloid Cells. J. Neurotrauma 36 (7), 1040–1053. [PubMed: 30259790]

Engelhardt B, Wolburg-Buchholz K, Wolburg H, 2001. Involvement of the choroid plexus in central nervous system inflammation. Microsc. Res. Tech. 52 (1), 112–129. [PubMed: 11135454]

Fabbri M, Paone A, Calore F, Galli R, Gaudio E, Santhanam R, Lovat F, Fadda P, Mao C, Nuovo GJ, Zanesi N, Crawford M, Ozer GH, Wernicke D, Alder H, Caligiuri MA, Nana-Sinkam P, Perrotti D, Croce CM, 2012. MicroRNAs bind to Toll-like receptors to induce prometastatic inflammatory response. Proc Natl Acad Sci U S A 109 (31), E2110–E2116. [PubMed: 22753494]

Feng Y, Chen H, Cai J, Zou L, Yan D, Xu G, Li D, Chao W, 2015. Cardiac RNA induces inflammatory responses in cardiomyocytes and immune cells via Toll-like receptor 7 signaling. J. Biol. Chem. 290 (44), 26688–26698. [PubMed: 26363072]

Feng Y, Zou L, Yan D, Chen H, Xu G, Jian W, Cui P, Chao W, 2017. Extracellular MicroRNAs Induce Potent Innate Immune Responses via TLR7/MyD88-Dependent Mechanisms. J. Immunol. 199 (6), 2106–2117. [PubMed: 28768728]

Fitzgerald KA, Kagan JC, 2020. Toll-like Receptors and the Control of Immunity. Cell 180 (6), 1044–1066. [PubMed: 32164908]

Fleischmann C, Scherag A, Adhikari NKJ, Hartog CS, Tsaganos T, Schlattmann P, Angus DC, Reinhart K, 2016. Assessment of Global Incidence and Mortality of Hospital-treated Sepsis. Current Estimates and Limitations. Am. J. Respir. Crit. Care Med. 193 (3), 259–272. [PubMed: 26414292]

Gasparotto J, Girardi CS, Somensi N, Ribeiro CT, Moreira JCF, Michels M, Sonai B, Rocha M, Steckert AV, Barichello T, Quevedo J, Dal-Pizzol F, Gelain DP, 2018. Receptor for advanced glycation end products mediates sepsis-triggered amyloid-beta accumulation, Tau phosphorylation, and cognitive impairment. J. Biol. Chem. 293, 226–244. [PubMed: 29127203]

Glass CK, Saijo K, Winner B, Marchetto MC, Gage FH, 2010. Mechanisms underlying inflammation in neurodegeneration. Cell 140 (6), 918–934. [PubMed: 20303880]

Gofton TE, Young GB, 2012. Sepsis-associated encephalopathy. Nat. Rev. Neurol. 8 (10), 557–566. [PubMed: 22986430]

Hanke M, Hoefig K, Merz H, Feller AC, Kausch I, Jocham D, Warnecke JM, Sczakiel G, 2010. A robust methodology to study urine microRNA as tumor marker: microRNA-126 and microRNA-182 are related to urinary bladder cancer. Urol. Oncol. 28 (6), 655–661. [PubMed: 19375957]

Hotchkiss RS, Moldawer LL, Opal SM, Reinhart K, Turnbull IR, Vincent JL, 2016. Sepsis and septic shock. Nat. Rev. Dis. Primers 2, 16045. [PubMed: 28117397]

Jeyaram A, Lamichhane TN, Wang S, Zou L, Dahal E, Kronstadt SM, Levy D, Parajuli B, Knudsen DR, Chao W, Jay SM, 2020. Enhanced Loading of Functional miRNA Cargo via pH Gradient Modification of Extracellular Vesicles. Mol. Ther. 28 (3), 975–985. [PubMed: 31911034]

Jian W, Gu L, Williams B, Feng Y, Chao W, Zou L, 2019. Toll-like Receptor 7 Contributes to Inflammation, Organ Injury, and Mortality in Murine Sepsis. Anesthesiology 131, 105–118. [PubMed: 31045897]

Khan NZ, Cao T, He J, Ritzel RM, Li Y, Henry RJ, Colson C, Stoica BA, Faden AI, Wu J, 2021. Spinal cord injury alters microRNA and CD81+ exosome levels in plasma extracellular nanoparticles with neuroinflammatory potential. Brain Behav. Immun. 92, 165–183. [PubMed: 33307173]

Kosaka N, Izumi H, Sekine K, Ochiya T, 2010. microRNA as a new immune-regulatory agent in breast milk. Silence 1, 7. [PubMed: 20226005]

Kuriakose M, Rama Rao KV, Younger D, Chandra N, 2018. Temporal and Spatial Effects of Blast Overpressure on Blood-Brain Barrier Permeability in Traumatic Brain Injury. Sci. Rep. 8, 8681. [PubMed: 29875451]

Lawrie CH, Gal S, Dunlop HM, Pushkaran B, Liggins AP, Pulford K, Banham AH, Pezzella F, Boultwood J, Wainscoat JS, Hatton CSR, Harris AL, 2008. Detection of elevated levels of tumour-associated microRNAs in serum of patients with diffuse large B-cell lymphoma. Br. J. Haematol. 141 (5), 672–675. [PubMed: 18318758]

Lehmann SM, Krüger C, Park B, Derkow K, Rosenberger K, Baumgart J, Trimbuch T, Eom G, Hinz M, Kaul D, Habbel P, Kälin R, Franzoni E, Rybak A, Nguyen D, Veh R, Ninnemann O, Peters O, Nitsch R, Heppner FL, Golenbock D, Schott E, Ploegh HL, Wulczyn FG, Lehnardt S, 2012. An unconventional role for miRNA: let-7 activates Toll-like receptor 7 and causes neurodegeneration. Nat. Neurosci. 15 (6), 827–835. [PubMed: 22610069]

Li Y, Ritzel RM, He J, Cao T, Sabirzhanov B, Li H, Liu S, Wu L-J, Wu J, 2021. The voltage-gated proton channel Hv1 plays a detrimental role in contusion spinal cord injury via extracellular acidosis-mediated neuroinflammation. Brain Behav. Immun. 91, 267–283. [PubMed: 33039662]

Li Y, Ritzel RM, Khan N, Cao T, He J, Lei Z, Matyas JJ, Sabirzhanov B, Liu S, Li H, Stoica BA, Loane DJ, Faden AI, Wu J, 2020. Delayed microglial depletion after spinal cord injury reduces chronic inflammation and neurodegeneration in the brain and improves neurological recovery in male mice. Theranostics 10 (25), 11376–11403. [PubMed: 33052221]

Lino MM, Simões S, Tomatis F, Albino I, Barrera A, Vivien D, Sobrino T, Ferreira L, 2021. Engineered extracellular vesicles as brain therapeutics. J. Control. Release 338, 472–485. [PubMed: 34428481]

Martin M, Rehani K, Jope RS, Michalek SM, 2005. Toll-like receptor-mediated cytokine production is differentially regulated by glycogen synthase kinase 3. Nat. Immunol. 6 (8), 777–784. [PubMed: 16007092]

Matyas JJ, O'Driscoll CM, Yu L, Coll-Miro M, Daugherty S, Renn CL, Faden AI, Dorsey SG, Wu J, 2017. Truncated TrkB.T1-Mediated Astrocyte Dysfunction Contributes to Impaired Motor Function and Neuropathic Pain after Spinal Cord Injury. J. Neurosci. 37 (14), 3956–3971. [PubMed: 28270575]

McCoy MK, Tansey MG, 2008. TNF signaling inhibition in the CNS: implications for normal brain function and neurodegenerative disease. J. Neuroinflamm. 5 (1), 45. 10.1186/1742-2094-5-45.

Mina F, Comim CM, Dominguini D, Cassol OJ Jr., Dall Igna DM, Ferreira GK, Silva MC, Galant LS, Streck EL, Quevedo J, Dal-Pizzol F, 2014. Il1-beta involvement in cognitive impairment after sepsis. Mol. Neurobiol. 49, 1069–1076. [PubMed: 24234155]

Mitchell PS, Parkin RK, Kroh EM, Fritz BR, Wyman SK, Pogosova-Agadjanyan EL, Peterson A, Noteboom J, O'Briant KC, Allen A, Lin DW, Urban N, Drescher CW, Knudsen BS, Stirewalt DL, Gentleman R, Vessella RL, Nelson PS, Martin DB, Tewari M, 2008. Circulating microRNAs as stable blood-based markers for cancer detection. PNAS 105 (30), 10513–10518. [PubMed: 18663219]

Moraes CA, Santos G, de Sampaio e Spohr TC, D'Avila JC, Lima FR, Benjamim CF, Bozza FA, Gomes FC, 2015. Activated Microglia-Induced Deficits in Excitatory Synapses Through IL-1beta: Implications for Cognitive Impairment in Sepsis. Mol. Neurobiol. 52, 653–663. [PubMed: 25257696]

Moy SS, Nadler JJ, Perez A, Barbaro RP, Johns JM, Magnuson TR, Piven J, Crawley JN, 2004. Sociability and preference for social novelty in five inbred strains: an approach to assess autistic-like behavior in mice. Genes Brain Behav. 3, 287–302. [PubMed: 15344922]

Muenzer JT, Davis CG, Dunne BS, Unsinger J, Dunne WM, Hotchkiss RS, 2006. Pneumonia after cecal ligation and puncture: a clinically relevant "two-hit" model of sepsis. Shock 26, 565–570. [PubMed: 17117130]

Park Chul-Kyu, Xu Zhen-Zhong, Berta Temugin, Han Qingjian, Chen Gang, Liu Xing-Jun, Ji Ru-Rong, 2014. Extracellular microRNAs activate nociceptor neurons to elicit pain via TLR7 and TRPA1. Neuron 82 (1), 47–54. [PubMed: 24698267]

Rittirsch Daniel, Huber-Lang, Markus S, Flierl, Ward Michael A, Peter A, 2009. Immunodesign of experimental sepsis by cecal ligation and puncture. Nat. Protoc. 4 (1), 31–36. [PubMed: 19131954]

Ritzel Rodney M., He Junyun, Li Yun, Cao Tuoxin, Khan Niaz, Shim Bosung, Sabirzhanov Boris, Aubrecht Taryn, Stoica Bogdan A., Faden Alan I., Wu Long-Jun, Wu Junfang, 2021. Proton extrusion during oxidative burst in microglia exacerbates pathological acidosis following traumatic brain injury. Glia 69 (3), 746–764. [PubMed: 33090575]

Ritzel Rodney M., Li Yun, He Junyun, Khan Niaz, Doran Sarah J., Faden Alan I., Wu Junfang, 2020. Sustained neuronal and microglial alterations are associated with diverse neurobehavioral dysfunction long after experimental brain injury. Neurobiol. Dis. 136, 104713. 10.1016/j.nbd.2019.104713. [PubMed: 31843705]

Roers Axel, Hiller Björn, Hornung Veit, 2016. Recognition of Endogenous Nucleic Acids by the Innate Immune System. Immunity 44 (4), 739–754. [PubMed: 27096317]

Sabirzhanov B, Zhao Z, Stoica BA, Loane DJ, Wu J, Borroto C, Dorsey SG, Faden AI, 2014. Downregulation of miR-23a and miR-27a following experimental traumatic brain injury induces neuronal cell death through activation of proapoptotic Bcl-2 proteins. J. Neurosci. 34, 10055–10071. [PubMed: 25057207]

Santos-Junior NN, Catalao CHR, Costa LHA, Souza AO, Mota CMD, Alberici LC, Branco LGS, Rocha MJA, 2018. Experimental sepsis induces sustained inflammation and acetylcholinesterase activity impairment in the hypothalamus. J. Neuroimmunol. 324, 143–148. [PubMed: 30190086]

Schroder J, Kahlke V, Staubach KH, Zabel P, Stuber F, 1998. Gender differences in human sepsis. Arch. Surg. 133, 1200–1205. [PubMed: 9820351]

Schwalm MT, Pasquali M, Miguel SP, Dos Santos JP, Vuolo F, Comim CM, Petronilho F, Quevedo J, Gelain DP, Moreira JC, Ritter C, Dal-Pizzol F, 2014. Acute brain inflammation and oxidative

damage are related to long-term cognitive deficits and markers of neurodegeneration in sepsis-survivor rats. Mol. Neurobiol. 49, 380–385. [PubMed: 23990375]

Shimada A, Hasegawa-Ishii S, 2021. Increased cytokine expression in the choroid plexus stroma and epithelium in response to endotoxin-induced systemic inflammation in mice. Toxicol. Rep. 8, 520–528. [PubMed: 33747797]

Shimada BK, Yang Y, Zhu J, Wang S, Suen A, Kronstadt SM, Jeyaram A, Jay SM, Zou L, Chao W, 2020. Extracellular miR-146a-5p Induces Cardiac Innate Immune Response and Cardiomyocyte Dysfunction. Immunohorizons 4, 561–572. [PubMed: 32958516]

Simi A, Tsakiri N, Wang P, Rothwell NJ, 2007. Interleukin-1 and inflammatory neurodegeneration. Biochem. Soc. Trans. 35, 1122–1126. [PubMed: 17956293]

Singer BH, Newstead MW, Zeng X, Cooke CL, Thompson RC, Singer K, Ghantasala R, Parent JM, Murphy GG, Iwashyna TJ, Standiford TJ, 2016. Cecal Ligation and Puncture Results in Long-Term Central Nervous System Myeloid Inflammation. PLoS ONE 11, e0149136. [PubMed: 26862765]

Singer M, Deutschman CS, Seymour CW, Shankar-Hari M, Annane D, Bauer M, Bellomo R, Bernard GR, Chiche JD, Coopersmith CM, Hotchkiss RS, Levy MM, Marshall JC, Martin GS, Opal SM, Rubenfeld GD, van der Poll T, Vincent JL, Angus DC, 2016. The Third International Consensus Definitions for Sepsis and Septic Shock (Sepsis-3). JAMA 315, 801–810. [PubMed: 26903338]

Sprung CL, Peduzzi PN, Shatney CH, Schein RM, Wilson MF, Sheagren JN, Hinshaw LB, 1990. Impact of encephalopathy on mortality in the sepsis syndrome. The Veterans Administration Systemic Sepsis Cooperative Study Group. Crit. Care Med. 18, 801–806. [PubMed: 2379391]

Turchinovich A, Tonevitsky AG, Burwinkel B, 2016. Extracellular miRNA: A Collision of Two Paradigms. Trends Biochem. Sci. 41, 883–892. [PubMed: 27597517]

Varatharaj A, Galea I, 2017. The blood-brain barrier in systemic inflammation. Brain Behav. Immun. 60, 1–12. [PubMed: 26995317]

Weber JA, Baxter DH, Zhang S, Huang DY, Huang KH, Lee MJ, Galas DJ, Wang K, 2010. The microRNA spectrum in 12 body fluids. Clin. Chem. 56, 1733–1741. [PubMed: 20847327]

Widmann CN, Heneka MT, 2014. Long-term cerebral consequences of sepsis. Lancet Neurol. 13, 630–636. [PubMed: 24849863]

Williams B, Neder J, Cui P, Suen A, Tanaka K, Zou L, Chao W, 2019. Toll-like receptors 2 and 7 mediate coagulation activation and coagulopathy in murine sepsis. J. Thromb. Haemost. 17, 1683–1693. [PubMed: 31211901]

Wu J, Zhao Z, Kumar A, Lipinski MM, Loane DJ, Stoica BA, Faden AI, 2016. Endoplasmic Reticulum Stress and Disrupted Neurogenesis in the Brain Are Associated with Cognitive Impairment and Depressive-Like Behavior after Spinal Cord Injury. J. Neurotrauma 33, 1919–1935. [PubMed: 27050417]

Xin H, Li Y, Cui Y, Yang JJ, Zhang ZG, Chopp M, 2013. Systemic administration of exosomes released from mesenchymal stromal cells promote functional recovery and neurovascular plasticity after stroke in rats. J. Cereb. Blood Flow Metab. 33, 1711–1715. [PubMed: 23963371]

Xu J, Feng Y, Jeyaram A, Jay SM, Zou L, Chao W, 2018. Circulating Plasma Extracellular Vesicles from Septic Mice Induce Inflammation via MicroRNA- and TLR7-Dependent Mechanisms. J. Immunol. 201, 3392–3400. [PubMed: 30355788]

Zhang Z, Ohto U, Shibata T, Krayukhina E, Taoka M, Yamauchi Y, Tanji H, Isobe T, Uchiyama S, Miyake K, Shimizu T, 2016. Structural Analysis Reveals that Toll-like Receptor 7 Is a Dual Receptor for Guanosine and Single-Stranded RNA. Immunity 45, 737–748. [PubMed: 27742543]

Zou L, Feng Y, Chen YJ, Si R, Shen S, Zhou Q, Ichinose F, Scherrer-Crosbie M, Chao W, 2010. Toll-like receptor 2 plays a critical role in cardiac dysfunction during polymicrobial sepsis. Crit. Care Med. 38, 1335–1342. [PubMed: 20228680]

Zou L, Feng Y, Xu G, Jian W, Chao W, 2016. Splenic RNA and MicroRNA Mimics Promote Complement Factor B Production and Alternative Pathway Activation via Innate Immune Signaling. J. Immunol. 196, 2788–2798. [PubMed: 26889043]

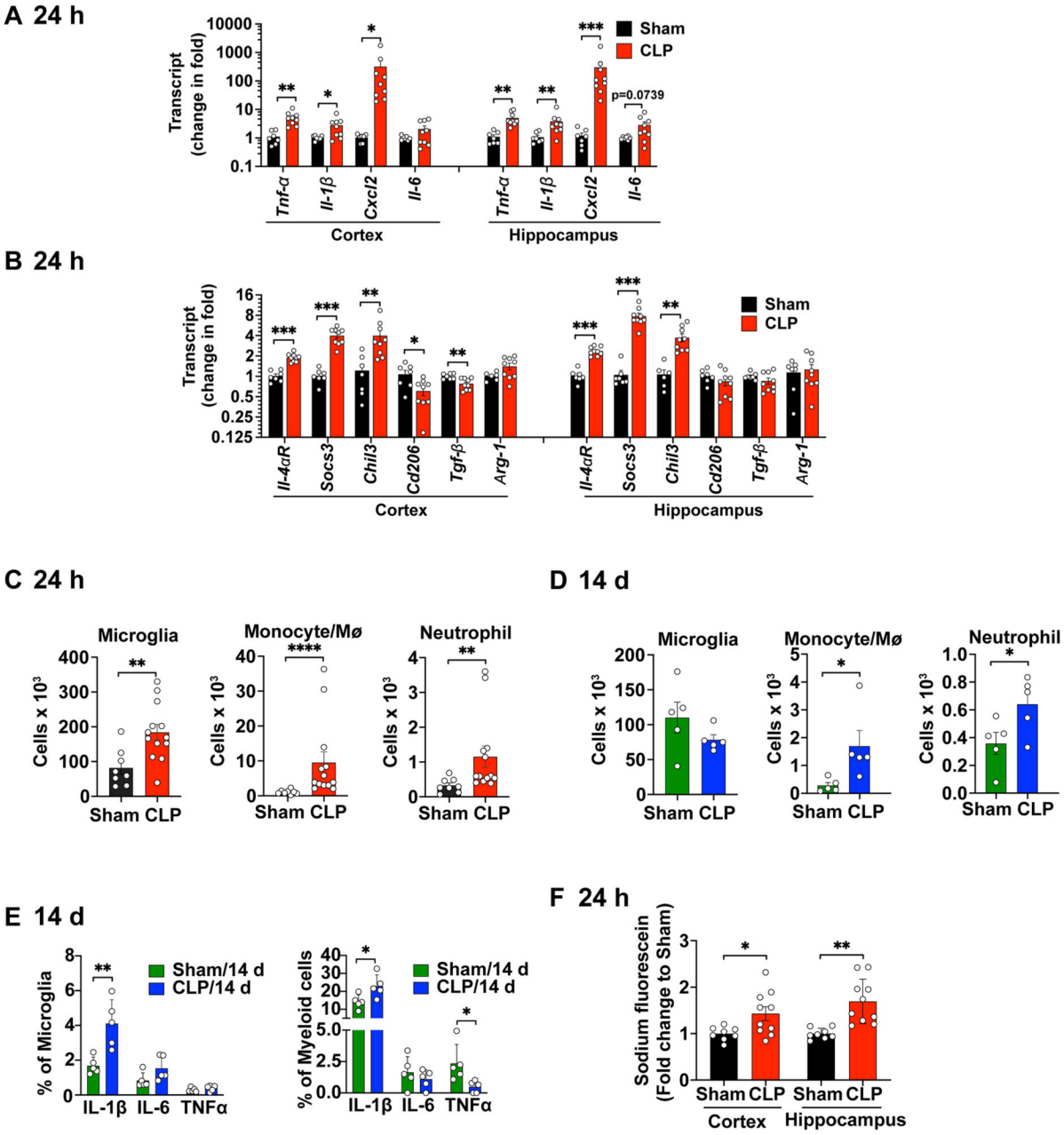

Fig. 1.

Brain inflammation and blood–brain barrier disruption in mice with polymicrobial sepsis. Mice were subjected to sham or CLP procedure, euthanized and brain tissue were collected at 24 h or 14 days after the surgical procedures. (A-B) Cytokine transcripts were tested in the cortex and hippocampus using Taqman qRT-PCR 24 h after sham or CLP. n = 7–9/group. $*p < 0.05$, $**p < 0.01$, $***p < 0.001$. *Cxcl2* was analyzed by Mann Whitney *U* test and the remaining cytokines were analyzed with unpaired *t*-test. (C) Flow cytometry analysis of brain microglia and monocytes/neutrophils 24 h after sham or CLP procedure. n = 8–13/group. $**p < 0.01$, unpaired *t* test. $****p < 0.0001$, Mann Whitney test. (D) Flow cytometry analysis of brain microglia and monocytes/neutrophils 14 days after sham or CLP procedure.

n = 5/group. *p = 0.0159 (Monocyte, Mann Whitney test), *p = 0.048 (Neutrophil, $t_{(8)}$ = 2.332, t test). (E) Percentage of microglia or myeloid cells expressing intracellular cytokine IL-1β, IL-6, and TNF-α at 14 days post procedure. n = 5/group. **p = 0.0058, $t_{(8)}$ = 3.723, unpaired t test; IL-1β, *p = 0.0299, $t_{(8)}$ = 2,636, unpaired t test; TNFα,*p = 0.0304, $t_{(8)}$ = 2,626, unpaired t test. (F) Blood-brain barrier permeability assessed by the leakage of sodium fluorescein from blood to brain tissue. n = 8–10/group. *p < 0.05, **p < 0.01, unpaired t-test.

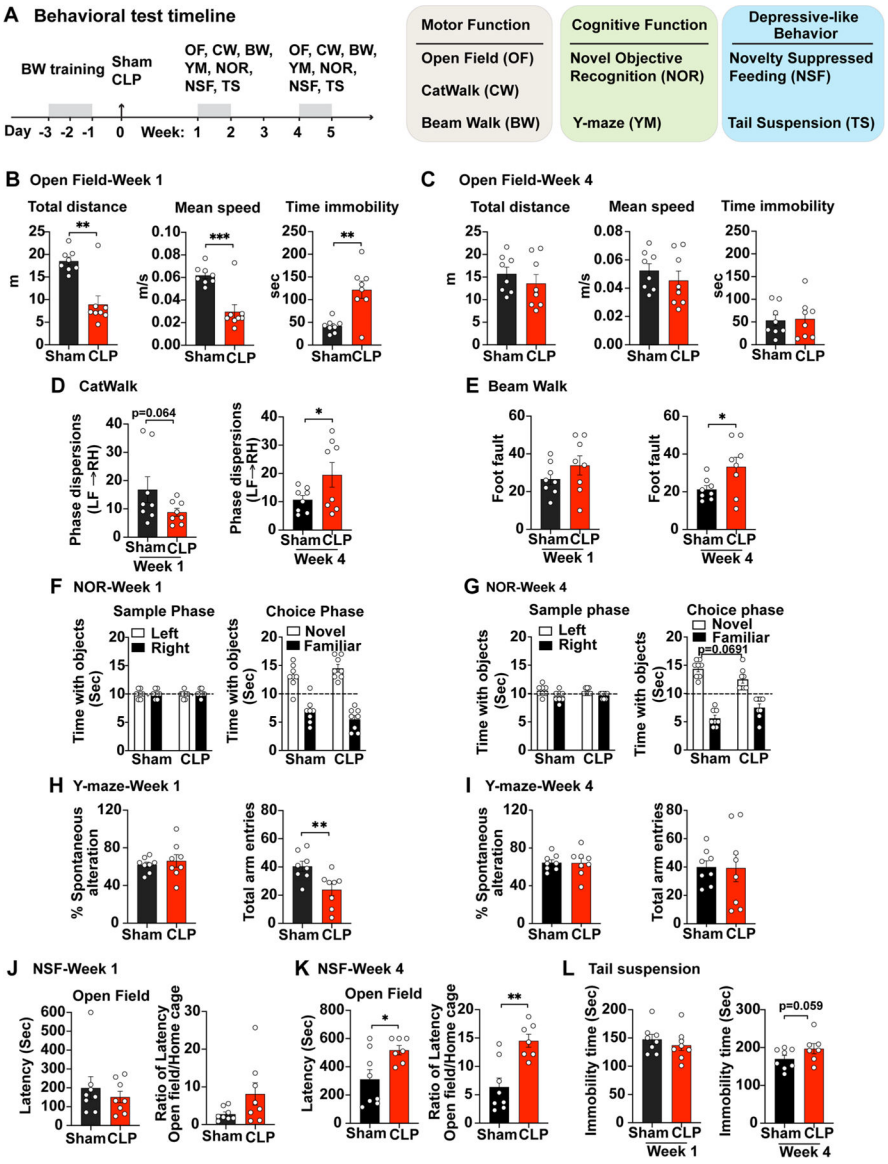

Fig. 2.

Sepsis induces functional impairment of the brain. (A) A schematic diagram of behavioral test timeline. Mice went through beam walk (BW) training for 2 consecutive days before they were subjected to sham or CLP procedure. A battery of behavioral tests to assess motor function, cognitive function, as well as feeding and stress behavior were performed at week 1 and 4 post-surgery. (B-C) Spontaneous locomotor activity was determined by Open Filed (OF). n = 8/group, $^{**}p < 0.01$, unpaired *t* test. (D) Gait analysis was evaluated by CatWalk (CW). Phase dispersion measures the coordinated walking pattern. n = 8/group, $^{*}p < 0.05$, unpaired *t* test. (E) Fine motor coordination and balance was tested by Beam Walk (BW). n = 8/group, $^{*}p < 0.05$, unpaired *t* test. (F-G) Non-spatial retention memory was tested by Novel Objective Recognition (NOR). Sample phase presents training stage. n = 8/group, $^{*}p < 0.05$, unpaired *t* test. (H-I) Hippocampus-dependent spatial working memory was evaluated by Y-maze. n = 8/group, $^{**}p < 0.01$, unpaired *t* test. (J-L) Rodent feeding and

stress behavioral performance was evaluated by Novelty Suppressed Feeding (NSF) and Tail suspension. n = 7–8/group, $*p < 0.05$, $**p < 0.01$, unpaired *t* test.

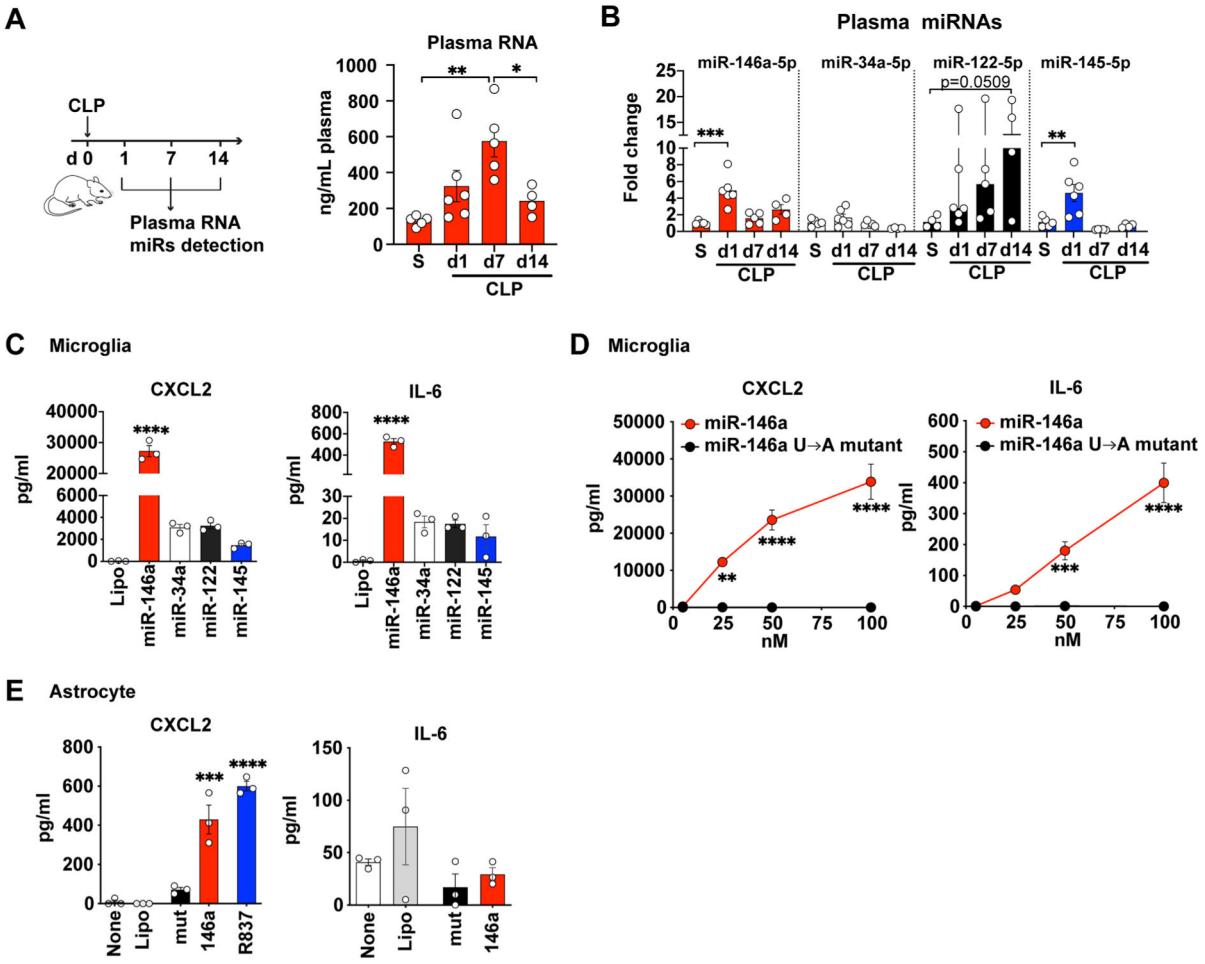

Fig. 3.

miRNA mimics induce cytokine production in both cultured microglia and astrocytes. (A) A schematic diagram of plasma collections following CLP and plasma RNA concentration at day 1, 7, 14. S = sham. n = 4–6/group. *$p = 0.0398$, **$p = 0.0026$, one-way ANOVA with Bonferroni *post hoc* test. (B) Relative expression of plasma miR-146a-5p, miR-34a-5p, miR-122–5p and miR-145–5p as normalized to spike in *cel*-miR-39 and expressed as fold change to the sham group (S). n = 4–6/group. Data represent mean ± SEM except miR-122 (Median, 95% CI). **$p = 0.0028$, ***$p = 0.0001$, one-way ANOVA with Bonferroni *post hoc* test and Kruskal-Wallis test for miR-122. (C) CXCL2 and IL-6 in microglia culture media following a 16–18 h treatment with 50 nM of various extracellular miRNAs. The experiments were repeated twice with triplicates. ****$p < 0.0001$, CXCL2: $F_{(4,10)} = 188.9$, IL-6: $F_{(4,10)} = 326.5$, one-way ANOVA with Bonferroni *post hoc* test. (D) miR-146a but not its U → A mutant dose-dependently induced CXCL2 and IL-6 production in cultured microglia. The experiments were repeated twice with triplicates. ***$p = 0.0005$, ****$p <$ 0.001, two-way ANOVA with Bonferroni *post hoc* test. (E) CXCL2 and IL-6 following a 16–18 h treatment with miR-146a (50 nM), U → A mutant (mut, 50 nM), and R837 (TLR7 ligand, 1 μg/ml) in cultured astrocytes. The experiments were repeated twice with triplicates. ***$p = 0.001$, ****$p < 0.0001$, one-way ANOVA with Bonferroni *post hoc* test.

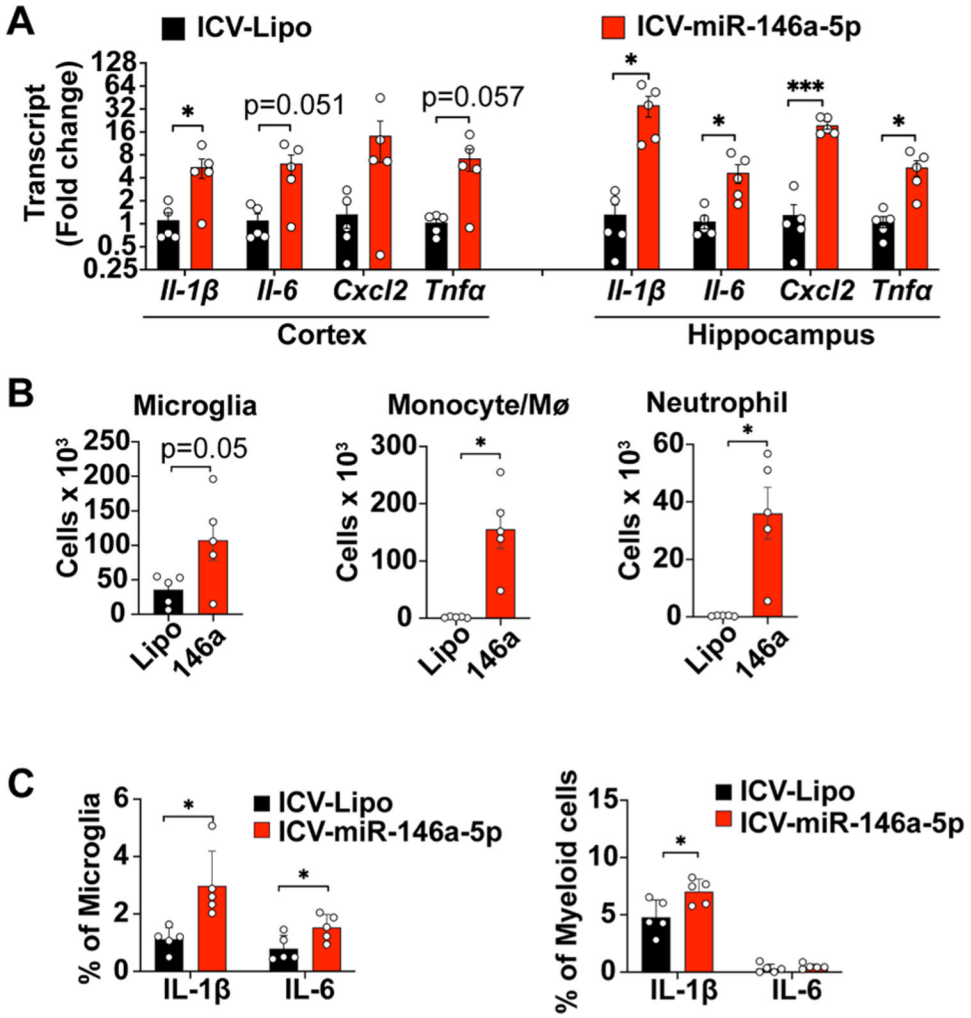

Fig. 4.

Intracerebroventricular (ICV) injection of miR-146a-5p causes neuroinflammation. A single dose of miR-146a-5p (5 μg) complexed with lipofectamine (Lipo) or Lipo alone was delivered *via* ICV injection to WT mice. Cytokine production and various innate immune cell populations in the brain were tested at 24 h. (A) Cytokine transcripts were tested in both the cerebral cortex and hippocampus. n = 5/group. Data represent mean ± SEM, $*p < 0.05$, $***p < 0.001$, unpaired *t*-test with Welch's correction. (B) Flow cytometry analysis of microglia, monocytes/macrophages, and neutrophils. $*p < 0.05$, unpaired *t* test with Welch's correction. (C) Percentage of microglia and myeloid cells expressing intracellular IL-1β and IL-6 as analyzed by flow cytometry. n = 5/group. $*p < 0.05$, unpaired *t* test.

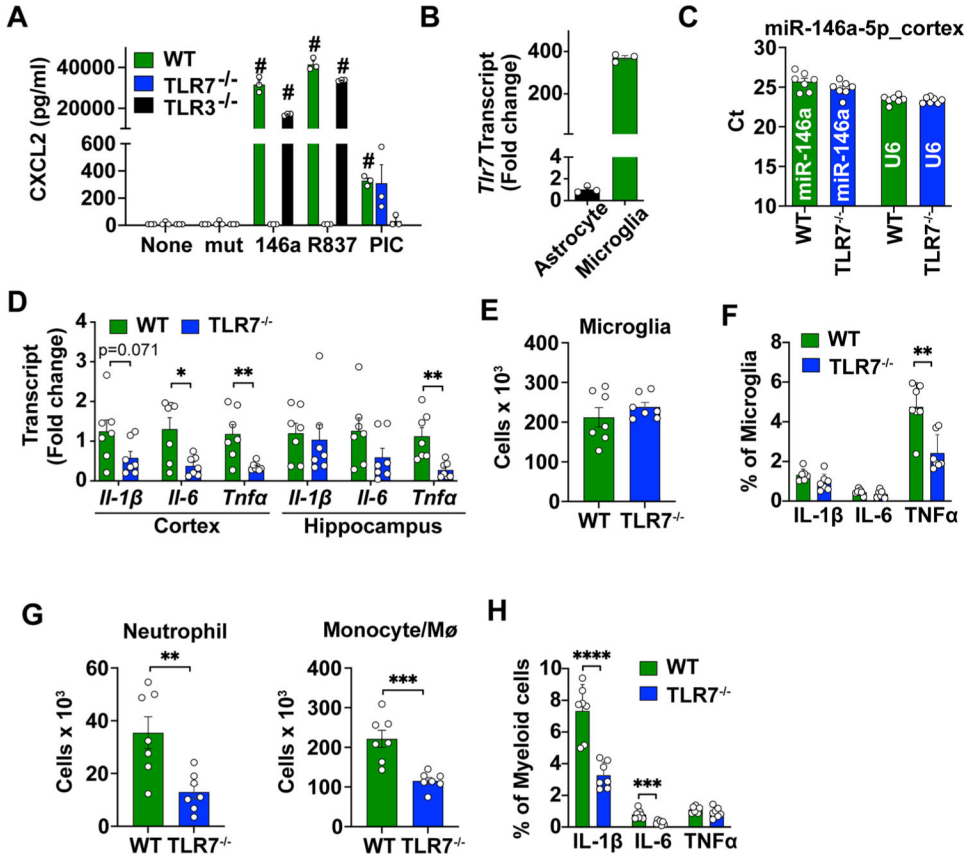

Fig. 5.

miR-146a-5p-induced neuroinflammation is lost in TLR7-deficient microglial cultures *in vitro* and in intact brain *in vivo*. (A) miR-146a-5p and R837-induced CXCL2 production was abolished in TLR7-deficient microglial cells. WT, TLR7$^{-/-}$, and TLR3$^{-/-}$ microglia were treated with lipofectamine-complexed miR-146a-5p mutant control (mut, 50 nM), miR-146a-5p (146a, 50 nM), the TLR7 ligand R837 (1 μg/ml), and the TLR3 ligand poly I:C (PIC, 10 μg/ml). CXCL2 in the media was assayed at 24 h with ELISA. n = 7/group. #$p < 0.001$ *vs.* None, two-way ANOVA with *post hoc* Bonferroni multiple comparison test was applied. (B) Relative expression levels of TLR7 transcript in microglia and astrocytes. The experiments were repeated twice with triplicates. n = 3/group. (C) miR-146a-5p expression in the cortex at 24 h after ICV (miR-146a: 5 μg) injection. n = 7/group. two-way ANOVA. (D) Cytokine transcripts in the cortex and hippocampus. n = 7/group, *$p < 0.05$, **$p < 0.01$, unpaired *t* test. (E) Flow cytometry analysis of microglia in WT and TLR7$^{-/-}$ mice at 24 h after miR-146a-5p (miR-146a: 5 μg) ICV injection. (F) Percentage of microglia expressing intracellular IL-1β, IL-6, TNFα as analyzed by flow cytometry. n = 7, **$p < 0.01$, unpaired *t* test. (G) Neutrophil and monocyte numbers in the brain. n = 7, **$p < 0.01$, ***$p < 0.001$, unpaired *t* test. (H) Percentage of myeloid cells expressing intracellular IL-1β, IL-6, TNFα as analyzed by flow cytometry. n = 7, ***$p < 0.001$, ****$p < 0.0001$, unpaired *t* test.

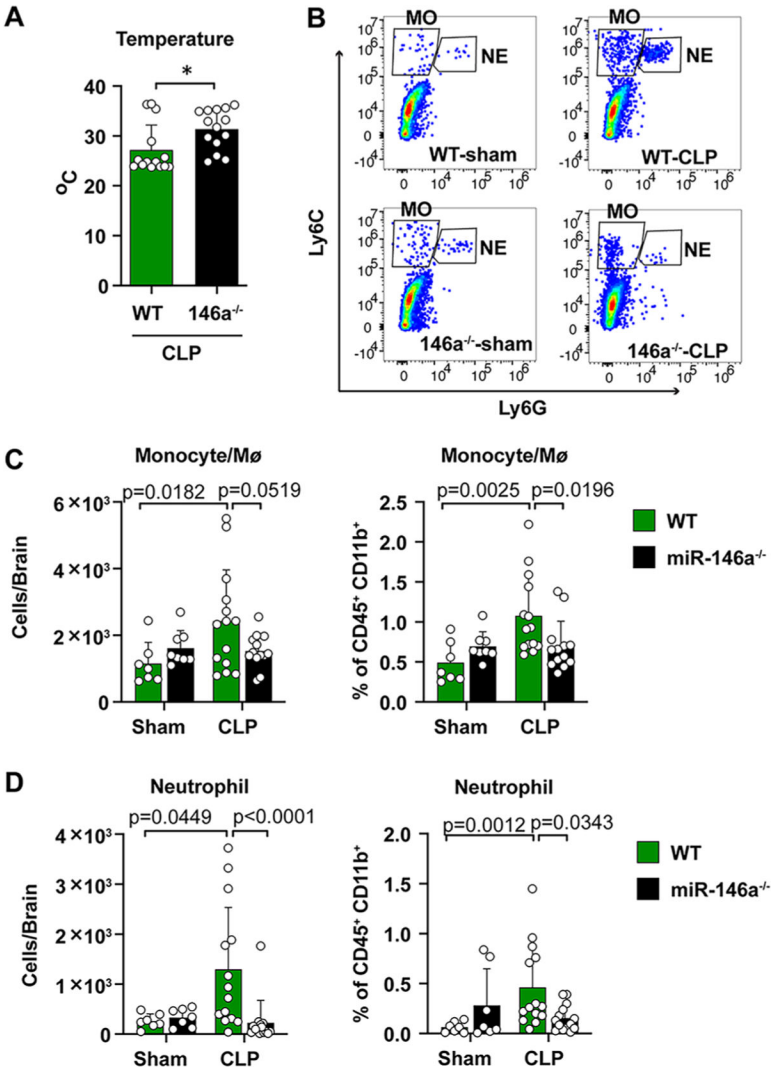

Fig. 6.

miR-146a deficiency reduces brain myeloid cell accumulation in sepsis. WT and miR-146a$^{-/-}$ mice were subjected to sham or CLP procedure. Body temperature, brain monocytes and neutrophils were evaluated at 24 h. (A) Rectal core temperature at 24 h. n = 14/group. *$p = 0.022$, *t* test. (B-D) Representative flow cytometry and quantitative numbers of brain neutrophils and monocytes at 24 h after sham/CLP in both WT and miR-146a$^{-/-}$ mice. n = 7–14/group. Two-way ANOVA with *post hoc* Bonferroni test.

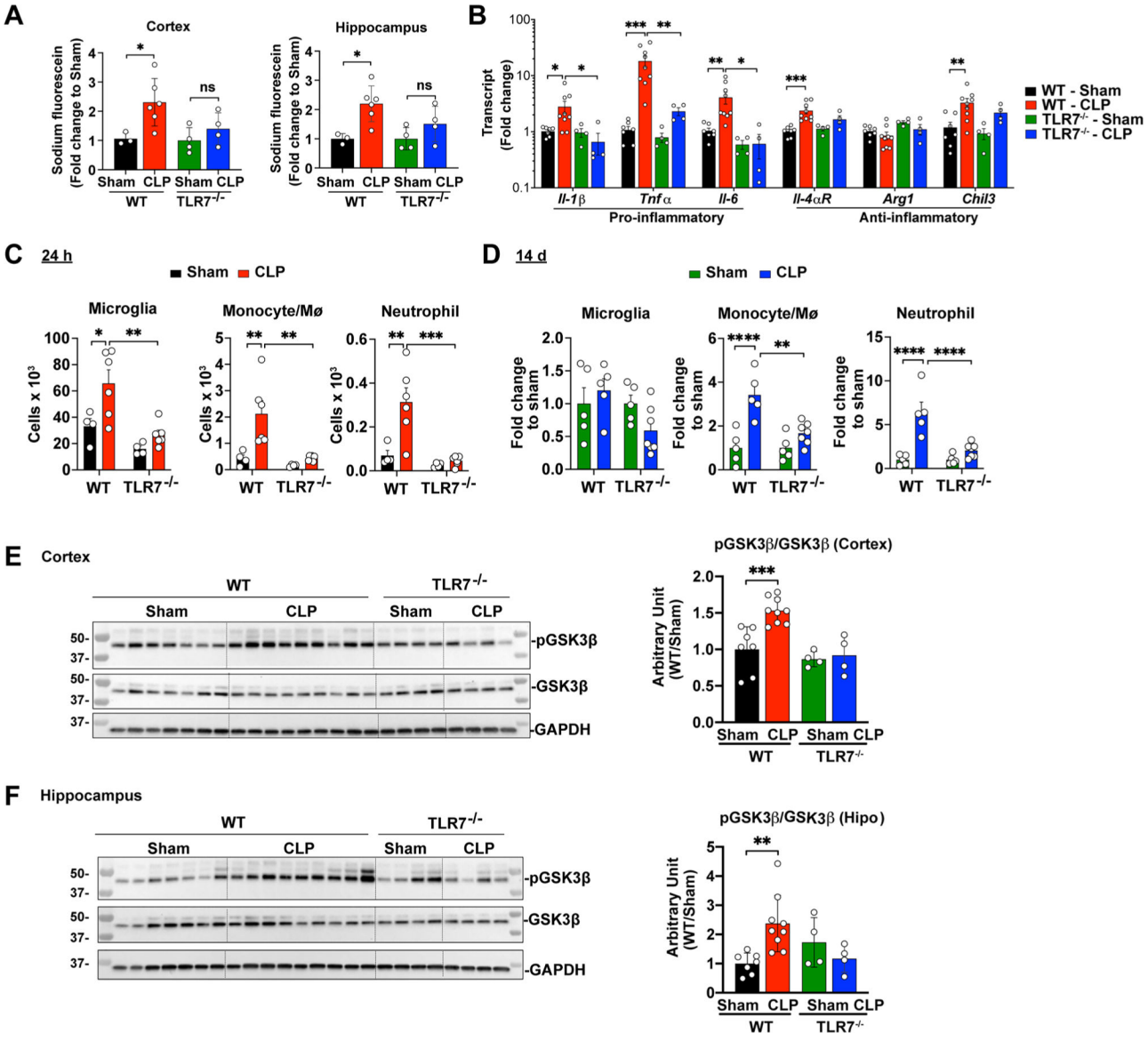

Fig. 7.

TLR7$^{-/-}$ mice have preserved BBB integrity and attenuated brain inflammation in sepsis. WT and TLR7$^{-/-}$ mice were subjected to sham or CLP procedure and brain tissue were collected at 24 h or 14 days. (A) BBB permeability as assessed by leakage of sodium fluorescein from blood to brain tissue at 24 h. n = 3–6/group. *$p < 0.05$, two-way ANOVA with *post hoc* Bonferroni test. (B) Cytokine gene expression in the cortex. n = 4–9/group. *$p < 0.05$, **$p < 0.01$, ***$p < 0.001$, two-way ANOVA with *post hoc* Bonferroni test. (C) Flow cytometry analysis of brain microglia, monocyte, and neutrophils at 24 h after sham/CLP in WT and TLR7$^{-/-}$ mice. n = 4–6/group. *$p < 0.05$, **$p < 0.01$, ***p < 0.001, two-way ANOVA with *post hoc* Bonferroni test. (D) Flow cytometry analysis of brain microglia, monocyte, and neutrophils at 14 days after sham/CLP in WT and TLR7$^{-/-}$ mice. n = 5–7/group. **$p < 0.01$, ****$p < 0.0001$, two-way ANOVA with *post hoc* Bonferroni test. (E) CLP led to an increased GSK3β phosphorylation in the cortex and hippocampus of WT, but

not that of TLR7$^{-/-}$ mice. Hippo = hippocampus. n = 4–9/group. **$p < 0.01$, ***$p < 0.001$, two-way ANOVA with *post hoc* Bonferroni test.

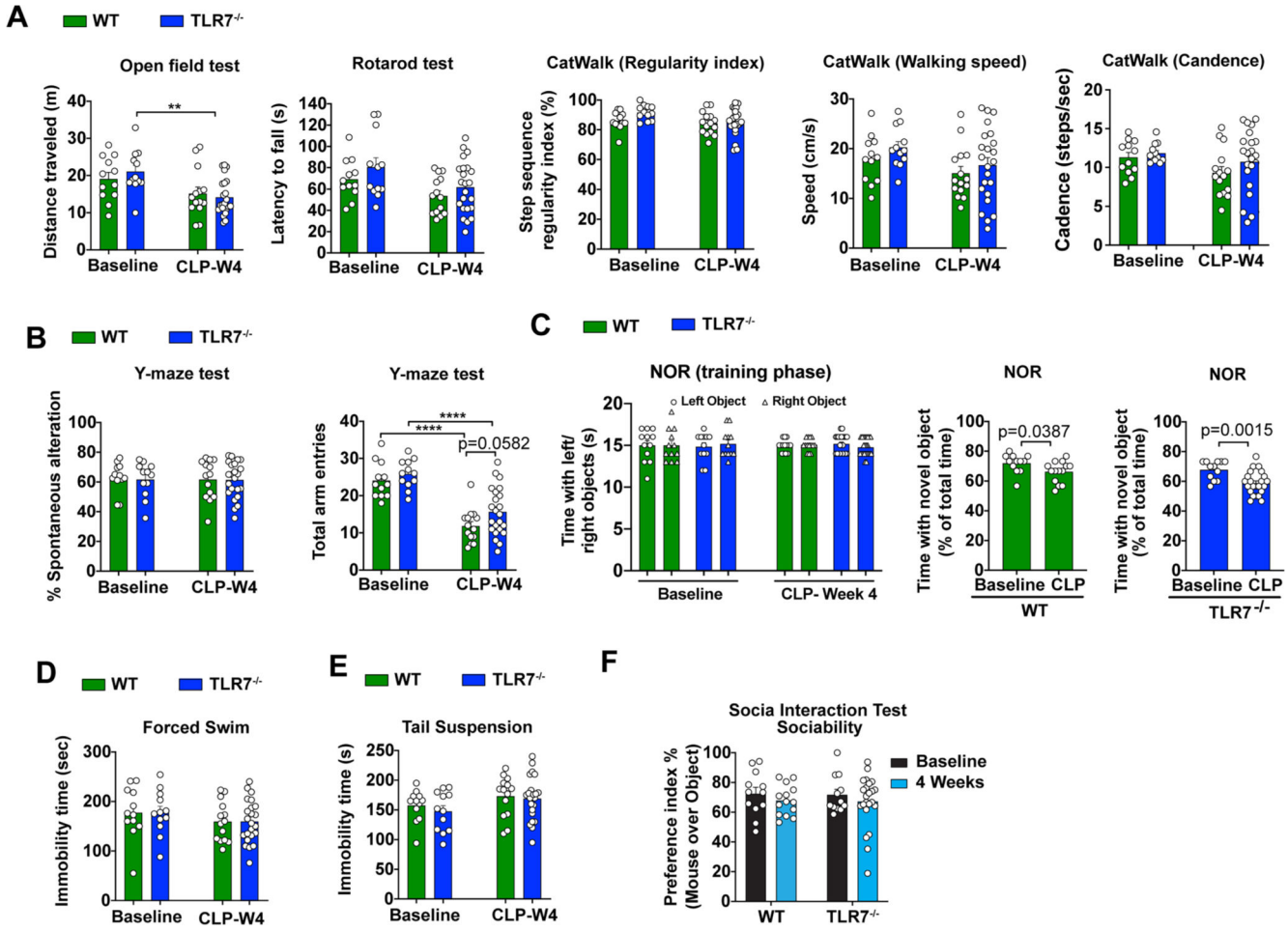

Fig. 8.

TLR7 deficiency has no impact on neurological dysfunction induced by polymicrobial sepsis. Behavioral function at baseline were tested 2 weeks prior to CLP procedure and tested again 4 weeks after in WT and TLR7$^{-/-}$ mice. (A) Motor function was evaluated by Open Field, Rotarod, and CatWalk tests. n = 12–23/group, **p = 0.0063, $F_{(1,57)}$ = 13.25, two-way ANOVA with *post hoc* Bonferroni test. (B) Hippocampus-dependent spatial working memory was evaluated by Y-maze. n = 12–23/group. ****$p < 0.0001$, two-way ANOVA with *post hoc* Bonferroni test. (C) Non-spatial retention memory was tested by Novel Objective Recognition. n = 12–23/group. Two-way ANOVA. (D-E) The forced swim test and tail suspension test. n = 12–23/group. two-way ANOVA. (F) Social Interaction Test. n = 12–23/group. Two-way ANOVA with *post hoc* Bonferroni test.